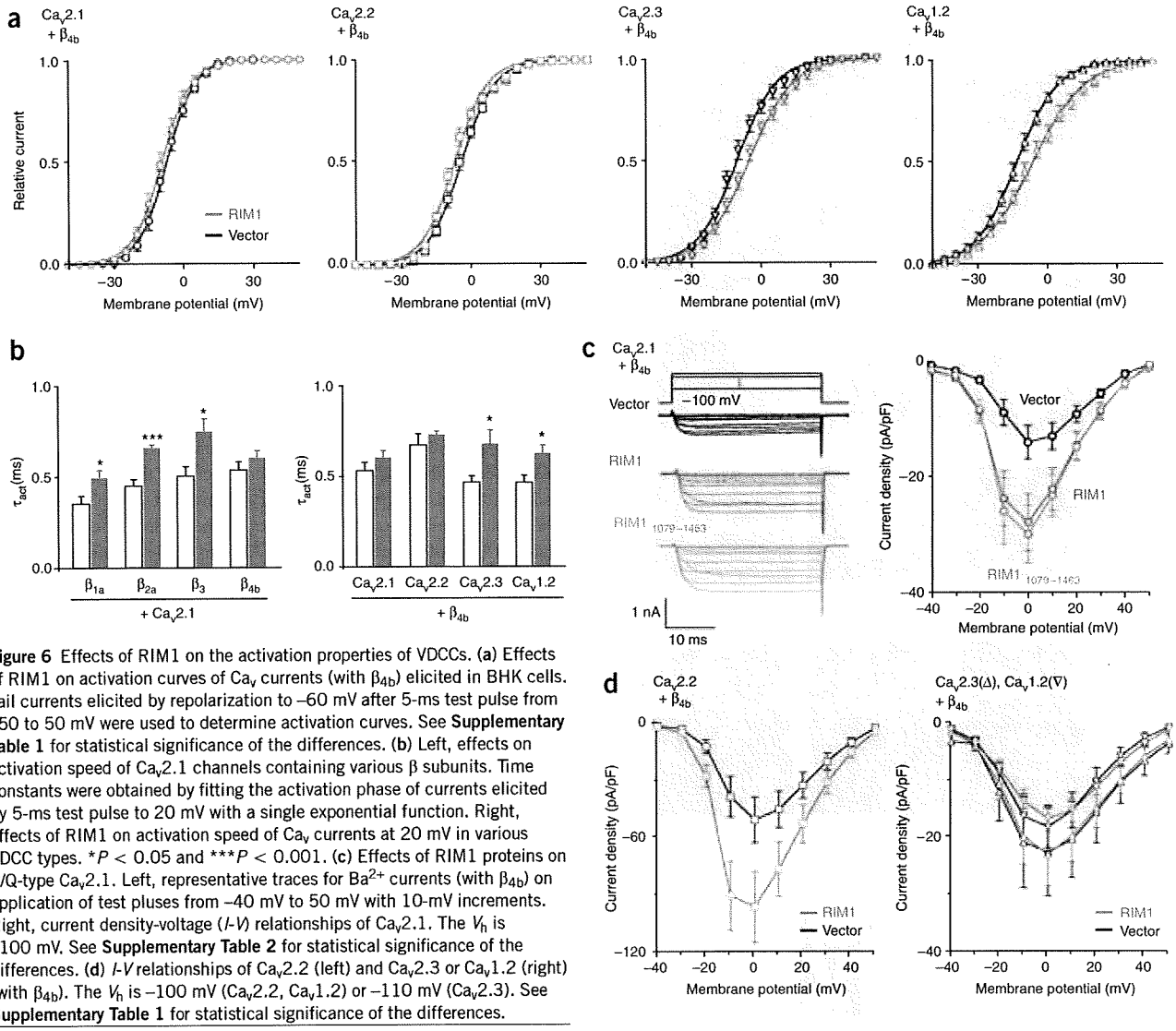

Figure 6 Effects of RIM1 on the activation properties of VDCCs. (**a**) Effects of RIM1 on activation curves of Ca_v currents (with β_{4b}) elicited in BHK cells. Tail currents elicited by repolarization to −60 mV after 5-ms test pulse from −50 to 50 mV were used to determine activation curves. See **Supplementary Table 1** for statistical significance of the differences. (**b**) Left, effects on activation speed of $Ca_v2.1$ channels containing various β subunits. Time constants were obtained by fitting the activation phase of currents elicited by 5-ms test pulse to 20 mV with a single exponential function. Right, effects of RIM1 on activation speed of Ca_v currents at 20 mV in various VDCC types. $*P < 0.05$ and $***P < 0.001$. (**c**) Effects of RIM1 proteins on P/Q-type $Ca_v2.1$. Left, representative traces for Ba^{2+} currents (with β_{4b}) on application of test pluses from −40 mV to 50 mV with 10-mV increments. Right, current density-voltage (*I-V*) relationships of $Ca_v2.1$. The V_h is −100 mV. See **Supplementary Table 2** for statistical significance of the differences. (**d**) *I-V* relationships of $Ca_v2.2$ (left) and $Ca_v2.3$ or $Ca_v1.2$ (right) (with β_{4b}). The V_h is −100 mV ($Ca_v2.2$, $Ca_v1.2$) or −110 mV ($Ca_v2.3$). See **Supplementary Table 1** for statistical significance of the differences.

RIM1-β interaction enhances neurotransmitter release

We studied the physiological relevance of RIM1 interactions with the VDCC complex by assessing neurotransmitter release from PC12 cells in which diverse high voltage–activated VDCC types have been precisely characterized[35,41] (**Supplementary Fig. 7** online). We transfected PC12 cells with RIM1 construct cDNAs along with *Chat* (encoding choline acetyltransferase), which synthesizes acetylcholine (ACh) for synaptic vesicles[42]. ACh release, triggered by Ca^{2+} influx in response to high-K^+ (elevation of extracellular K^+ concentration from 5.9 mM to 51.1 mM) membrane depolarization, was significantly potentiated by full-length RIM1 (**Fig. 8a** and **Supplementary Fig. 7**, $P < 0.001$). ACh release was also enhanced by the Rab3-interacting N-terminal $RIM1_{11–399}$ and by the C-terminal $RIM1_{1079–1463}$ that maintains VDCC currents, but not by the middle $RIM1_{400–1078}$. In contrast, BADN significantly suppressed ACh release ($P < 0.001$). In cultured cerebellar neurons, similar suppression by BADN and potentiation by the full-length RIM1 were observed for high K^+–induced glutamate release (**Fig. 8b**). The results suggest that RIM1 potentiates neurotransmitter release through its interaction with VDCC β in neuronal and neuron-like cells.

DISCUSSION

The present investigation reveals a previously unknown physical association between the presynaptic active zone proteins RIM1 and VDCC β subunits. The results of yeast two-hybrid assays, *in vitro* binding assays and coimmunoprecipitation experiments have identified a RIM1-VDCC complex formed by direct interaction of the β subunit with the α_1 subunit AID region and the RIM C terminus (residues 1079–1463) (**Fig. 1**). The identification of native RIM1-VDCC complexes in brain (**Fig. 2**), the colocalization of RIM1 with VDCC subunits at the plasma membrane and the presynapse, and the disruption of such localization and complex formation by BADN (**Fig. 3**) support a physiological role for the RIM1-β association. Further biochemical and functional analyses (**Figs. 1** and **4**) suggest that $RIM1_{1079–1257}$ and $RIM1_{1258–1463}$ are the primary β subunit binding site and modulatory region, respectively, in the RIM1 protein. Although our experiments showed that RIM1 and β_4 interacted, the RIM1 in wild-type brains was indistinguishable from that found in the brains of lethargic mice by sucrose gradient profile (**Fig. 2a,d**). It has been previously reported that the immunolocalization of $Ca_v2.1$ and $Ca_v2.2$ in the brain and the properties of P-type currents in Purkinje

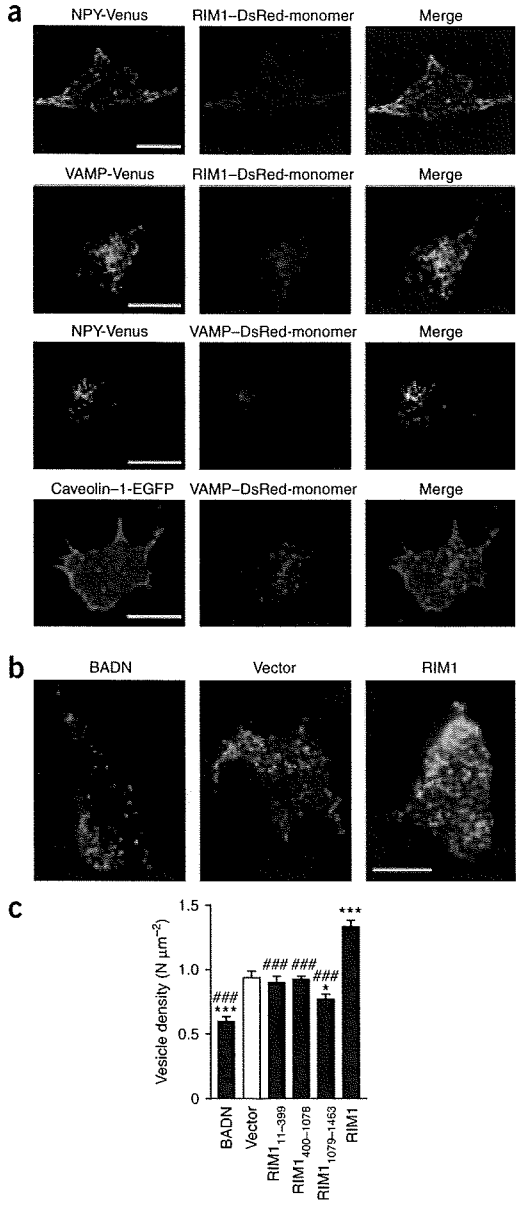

Figure 7 RIM1 and β subunits associate to anchor neurotransmitter vesicles to VDCCs at the plasma membrane. (**a**) NPY-containing secretory vesicles were colocalized with RIM1 and VAMP that was not colocalized with caveolin-1 in PC12 cells. NPY-Venus and RIM1–DsRed-monomer, VAMP-Venus and RIM1–DsRed-monomer, NPY-Venus and VAMP–DsRed-monomer, or caveolin-1–EGFP and VAMP–DsRed-monomer were coexpressed in PC12 cells and live images of the cells were obtained by confocal microscopy. Scale bar, 10 μm. (**b**,**c**) Effects of RIM1 constructs and BADN on the density of docked vesicles. Typical TIRF images of plasma membrane–docked vesicles containing NPY-Venus are shown in **b**. Left, BADN-cotransfected PC12 cell. Middle, vector-cotransfected PC12 cell. Right, RIM1-cotransfected PC12 cell. Scale bar, 10 μm. In **c**, the vesicle density was determined by counting the vesicles in each image ($n = 20$ cells in each). $^{*}P < 0.05$, $^{***}P < 0.001$ versus vector. $^{###}P < 0.001$ versus RIM1.

neurons are indistinguishable between wild-type and lethargic mice[32]. This has been attributed to the rescue of β_4 deficiency by the remaining subunits, β_1, β_2 and β_3. We expect a similar compensatory mechanism may also occur in the RIM1-β interaction in lethargic mice. Therefore, the β_4 isoform is unlikely to exclusively mediate the RIM1-VDCC association in the brain.

The RIM1-β association enables RIM1 to have a dual physiological function in neurotransmitter release: sustaining Ca^{2+} influx through the functional regulation of VDCCs and anchoring vesicles to VDCCs (**Supplementary Fig. 8** online). Among the functional parameters of VDCCs, those that are related to voltage-dependent inactivation are most prominently modified by RIM1 through the β interaction (**Fig. 4**). The inactivation kinetics are markedly decelerated, resulting in the predominance of high-voltage inactivation and an inactivation-resistant current component in the 2-s prepulse protocol. The similarly modulated inactivation properties of P/Q-type VDCCs by RIM2α, RIM3γ or RIM4γ (unpublished data), which all carry the C_2B domain, suggest that this function is a common feature for the RIM family[5]. Suppression by BADN of the RIM1-mediated inactivation in both the recombinant (**Supplementary Fig. 5**) and native VDCCs (**Fig. 5c**) provides evidence that RIM1 exerts observed effects through the RIM1-β association. This is supported by our finding that β_4-GK, which binds to α_1 (ref. 37) but not to RIM1, did not mediate RIM1 effects on N-type channels (**Supplementary Fig. 5**). Although the detailed molecular mechanisms underlying inactivation have yet to be determined, previous mapping of the molecular determinants for voltage-dependent inactivation kinetics[43] suggest that RIM1-β complexes bound to the I-II linker AID further act on adjacent segment S6 of repeat I to hinder its conformational transition to the inactivated state. Alternatively, RIM1 may immobilize the β subunit and the process of inactivation by slowing the movement of the I-II loop[44,45]. When voltage-dependent inactivation is thus suppressed, the responses of Ca^{2+} sensors such as synaptotagmins to Ca^{2+} influx may be potentiated at depolarizing membrane potentials that induce voltage-dependent inactivation when RIM1 is absent. Because RIM1 virtually abolished VDCC inactivation that was elicited by a train of action potential waveforms (**Fig. 4f**), certain forms of synaptic depression via closed-state inactivation[36] may be minimized by RIM1 at presynaptic active zones. The impact of the RIM1-β association on delaying VDCC inactivation may explain recent findings with the RIM1α knockout mouse showing that RIM1 is important for the late-stage asynchronous neurotransmitter release, whereas synaptotagmin I is involved in the earlier synchronous release[12]. With P/Q- and N-type channels, the RIM1-β association significantly affected channel activity as well; current densities were nearly doubled by RIM (**Fig. 6c**). Thus, RIM1 can maintain and enhance depolarization-induced Ca^{2+} influx to support neurotransmitter release at presynaptic active zones.

Regarding the role of RIM1 in vesicle anchoring to VDCC at the plasma membrane, full-length RIM1 is required to mediate vesicle anchoring, in contrast to the RIM1 suppression of VDCC inactivation, which requires only the RIM1 C terminus. Taking into consideration the direct RIM1-Rab3 association and the regulation of tethering and/or priming of synaptic vesicles by Rab3 (ref. 40), it is likely that simultaneous interactions of RIM1 with vesicle-associated Rab3 and Munc13 via the N-terminal Zn^{2+}-finger domain and with the VDCC β subunit via the C-terminal C_2B domain underlie, at least in part, the maintenance of the close proximity of VDCCs to vesicles, thereby regulating the dynamic properties of synaptic transmission[3]. Supporting this idea, BADN and $RIM1_{1079–1463}$ significantly suppressed vesicle docking in PC12 cells (**Fig. 7c**). In our experiments, however, RIM1 and β subunit targeting to the presynaptic site was observed only after early synapse formation (**Fig. 3**). It is possible that the interaction of Mint and CASK with VDCC α_1 subunits via their C termini[22,23] may

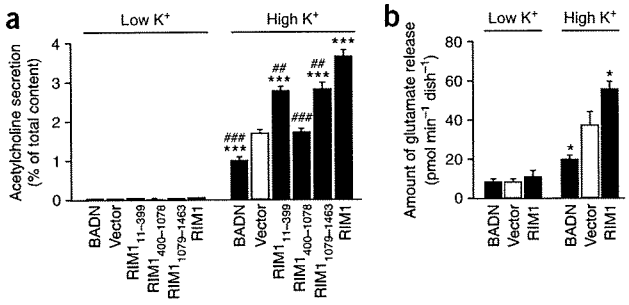

Figure 8 The RIM1-β association enhances neurotransmitter release in PC12 cells and cultured cerebellar neurons. (**a**) Effects of RIM1 constructs and BADN on depolarization-dependent release of ACh from ChAT-cotransfected PC12 cells. Three days after transfection, PC12 cells were incubated for 30 s with low-K^+ solution (5.9 mM K^+) at 37 °C. The release of ACh during this period was considered to be basal release. To measure ACh release, the cells were then incubated for 30 s with a high-K^+ solution (51.1 mM K^+). The amount of secreted ACh was determined as a percentage of the cellular content for each dish. $^{***}P < 0.001$ versus vector. $^{\#\#}P < 0.01$, $^{\#\#\#}P < 0.001$ versus RIM1. (**b**) Effects of RIM1 and BADN on depolarization-dependent release of glutamate from cultured cerebellar neurons. Twenty-four hours after the introduction of cDNAs, cerebellar neurons (9–11 DIV) were incubated for 1 min with the low-K^+ solution (5.9 mM K^+) at 37 °C. The release of glutamate during this period was considered to be basal release. To measure glutamate release, the cells were then incubated for 1 min with a high-K^+ solution (51.1 mM K^+). $^*P < 0.05$.

also direct channel targeting in parallel of, or before, RIM1–β subunit complex formation. Notably, our observation is consistent with a previous report[46] stating that the loss of the RIM homolog UNC10 caused a reduction in membrane-contacting synaptic vesicles within 30 nm of the dense projection at *Caenorhabditis elegans* neuromuscular junctions. Furthermore, in RIM1α-deficient mice, the decay of excitatory postsynaptic currents (EPSCs) during 14-Hz trains of presynaptic stimulation is abolished, whereas the rate at which the readily releasable vesicle pool is refilled is indistinguishable between the wild-type and RIM1α mutant mice[12]. These data suggest that RIM1-mediated vesicles anchoring to VDCCs may enable a rapid depletion of vesicle pools such that the available vesicles are exhausted, leading to EPSC decay. In this scenario, RIM1 knockout would minimize rapid vesicle release, enabling the readily releasable pool to be maintained and thus prevent EPSC decay. More recently, it has been reported that mice deficient in both RIM1α and RIM2α show lethality due to defects in Ca^{2+}-triggered release despite normal presynaptic active zone length and normal spontaneous neurotransmitter release[47]. In combination, these studies support our model (**Supplementary Fig. 8**), predicting a dual function for the RIM1-β interaction in neurotransmitter release by coordinating the molecular constituents and Ca^{2+} signaling in presynaptic active zones.

Previous reports have demonstrated the functional impact of syntaxin, synaptosome-associated protein (SNAP-25) and synaptotagmin on VDCCs through physical association with the 'synprint' region in the II-III linker of α_1-proteins[19–21]. It has been reported[48] that RIM associates with the synprint[10] directly via the C_2A domain, and with the α_1 C-terminal tail indirectly via the RIM-binding protein (RIM-BP) (**Fig. 1a**). However, RIM1 regulation of VDCCs may be independent of the synprint- or RIM-BP–mediated association, because $RIM1_{1079–1463}$, which lacks both the C_2A domain necessary for synprint binding[10] and the PXXP motif for the RIM-BP binding, is still sufficient to inhibit VDCC inactivation (**Fig. 4a,c**). This is supported by our observation that BADN, or replacement of β with β_4-GK, was sufficient to disrupt the RIM1 effects on inactivation (**Supplementary Fig. 5**). Syntaxin and SNAP-25 have been proposed to inhibit VDCC-mediated Ca^{2+} influx via a hyperpolarizing shift of the inactivation curve in the absence of vesicle docking at VDCC sites[19,21], whereas our finding implies enhancement or maintenance of the Ca^{2+} influx via interaction with RIM1 during the docking of vesicles. Notably, previous reports suggest that RIM1 is involved in the modification of the release apparatus at a late stage in the vesicle cycle[9], particularly in the postdocking step[49]. In early phases of vesicle docking, VDCC α_1 interactions with syntaxin and SNAP25 (refs. 19–21) and Mint and CASK[22,23] may be important, eliciting partial resistance to BADN suppression of vesicle docking (**Fig. 7c**). Thus, the α_1 protein associations and the RIM1-β association may be distinct interactions that contribute at different stages of vesicle cycling to controlling the Ca^{2+} supply from the source, namely the VDCC, in addition to regulating the proximity between the Ca^{2+} source VDCC and the target Ca^{2+} sensors at the presynaptic active zone.

METHODS

cDNA expression, cell culture, molecular modeling, recombinant proteins and infection with Sindbis viruses. Methods for cDNA cloning and expression, cell culture, molecular modeling of BADN, preparation of GST fusion proteins and purified β_{4b}-subunit recombinants, and the preparation and infection of Sindbis viruses can be found in the **Supplementary Methods** online.

Yeast two-hybrid screening and β-galactosidase assay. We subcloned rat β_{4b} subunit (GenBank accession number XM_215742) into pGBK-T7 and used it as a bait to screen a mouse brain pACT2 library in the yeast strain AH109 (Clontech). We plated transformants (1.5×10^6) on synthetic medium lacking adenine, histidine, leucine and tryptophan and assayed His^+ colonies for β-galactosidase activity with a filter assay. Of the transformants, 103 were His^+, and 21 of these were also $LacZ^+$. We isolated prey clone no. 2–5, encoding $RIM1_{1079–1463}$ (NM_053270).

***In vitro* binding of the purified proteins, GST-pulldown and coimmunoprecipitation experiments.** RIM1-GST fusion proteins at various concentrations were incubated with 50 pM purified recombinant β_4 subunits for 3 h at 4 °C. Proteins were subjected to western blotting with an antibody for β_4 raised against the peptide ENYHNERARKSRNRLS. The densities of protein signals, obtained using NIH Image (National Institute of Mental Health) under the linear relationship with the applied amount of proteins (**Supplementary Fig. 2**), were normalized to the densities from the maximal binding. For the pulldown assays, the cell lysate was incubated with glutathione-Sepharose beads bound to purified fusion proteins. The proteins were characterized by western blotting with antibody for Myc (Invitrogen). For coimmunoprecipitation, the cell lysate was incubated with anti-FLAG M2 monoclonal antibody (Sigma), and the immunocomplexes were characterized by western blotting with antibody for Myc. For details, see **Supplementary Methods**.

Biochemistry of native neuronal VDCC complexes. VDCC complexes were partially purified from the brains of C57BL/6 or lethargic mice (B6EiC3Sn-*a/A-Cacnb4*^{lh}/J, Jackson Laboratory) as previously reported[25]. KCl washed microsomes (50 mg) were solubilized in buffer I (for buffers, see **Supplementary Table 8** online) and centrifuged at 142,000*g* for 37 min. The supernatant was incubated with heparin-agarose (Sigma); agarose was washed with buffer II and III before elution with buffer IV. After elution, samples were diluted to 150 mM NaCl by addition of buffer V and concentrated using centrifugal filter devices (Millipore). The samples were applied to 5–40% sucrose density gradients (buffer VI) and were centrifuged at 215,000*g* for 90 min. Western blots were performed using antibodies for RIM (BD Biosciences), $Ca_v2.1$ (Alamone), syntaxin (Sigma) and β_4 (described above). Western blot band densities (NIH image) were normalized from four to five independent experiments.

For immunoprecipitation, partially purified neuronal VDCC complexes were incubated with protein A–agarose coupled to antibodies for β_4 or RIM1[4]. Immunoprecipitated proteins were subject to western blotting with

antibodies for RIM or $Ca_v2.1$. To disrupt the physiological association of native RIM1 with VDCC β_4, partially purified VDCC complexes were incubated with 200 nM GST-BADN and GST-$RIM1_{1079–1463}$ for 8 h at 4 °C before immunoprecipitation.

Confocal imaging. At 32 h after transfection, HEK293 cells or PC12 cells were plated on poly-L-lysine–coated glass coverslips. Hoechst 33342 (1 μg ml^{-1}, Dojindo) was added to stain nuclei 56 h after transfection. The imaging was performed in modified Ringer's buffer that contained 130 mM NaCl, 3 mM KCl, 5 mM $CaCl_2$, 1.5 mM $MgCl_2$, 10 mM glucose and 10 mM HEPES (pH 7.4). Fluorescence images were acquired with a confocal laser-scanning microscope (FV500, Olympus). For details, see the **Supplementary Methods**.

TIRF imaging. PC12 cells cotransfected with 1 μg pVenus-N1-NPY and RIM1 expression plasmids at the equal molar quantity (5.0 μg $RIM1_{11–399}$, 5.7 μg $RIM1_{400–1078}$, 5.0 μg $RIM1_{1079–1463}$ or 7.5 μg RIM1) and BADN (10 μg) using OptiFect (Invitrogen) were plated onto poly-L-lysine–coated coverslips. PCR analysis showed that the RIM plasmids were transfected at the equal level (**Supplementary Fig. 7**). The imaging was performed in modified Ringer's buffer. Fluorescence images of NPY-Venus were taken at the single vesicle level using an inverted microscope (IX71, Olympus). Incident light for total internal reflection illumination was introduced from the high numerical objective lens through a single mode optical fiber. Images were captured by a cooled CCD camera (EM-CCD, Hamamatsu Photonics). Area calculations and fluorescent spot counting were performed using Metamorph software (Molecular Devices). The cells showing distribution of vesicles with <10 μm^2 dark circle area that can be placed in between vesicles were selected as cells with uniformly distributed vesicles. The maximal dark circle area in the images from BADN-transfected cells with uniform vesicle distribution was 10 μm^2. For details, see the **Supplementary Methods**.

Immunostaining of cultured hippocampal neurons. Culture and transfection of mouse hippocampal neurons were carried out as described[50]. EGFP-tagged $Ca_v2.1$, Myc-tagged RIM1 and FLAG-tagged β_{4b} were detected with a Zeiss LSM510META confocal microscope using a combination of antibodies: FLAG M2 monoclonal, Myc polyclonal (Cell Signaling) and Alexa488- and Alexa594-conjugated secondary antibodies (Invitrogen). See the **Supplementary Methods** for further quantification procedures.

Current recordings. Whole-cell mode of the patch-clamp technique was carried out at 22–25 °C. An external solution contained 3 mM $BaCl_2$, 155 mM tetraethylammonium chloride (TEA-Cl), 10 mM HEPES and 10 mM glucose for BHK cells, and 10 mM $BaCl_2$, 153 mM TEA-Cl, 10 mM HEPES and 10 mM glucose for PC12 cells (pH 7.4). The pipette solution contained 95 mM CsOH, 95 mM aspartate, 40 mM CsCl, 4 mM $MgCl_2$, 5 mM EGTA, 2 mM disodium ATP, 5 mM HEPES and 8 mM creatine phosphate (pH 7.2). To characterize Ca^{2+}-dependent inactivation, external solutions contained 5 mM $CaCl_2$ or $BaCl_2$, 153 mM TEA-Cl, 10 mM HEPES and 10 mM glucose (pH 7.4). The pipette solution contained 135 mM Cs-$MeSO_3$, 5 mM CsCl, 0.5 mM EGTA, 5 mM $MgCl_2$, 4 mM disodium ATP and 10 mM HEPES (pH 7.2). Single-channel currents were recorded using cell-attached patch mode. The bath solution contained 150 mM KCl, 5 mM HEPES, 0.2 mM EGTA and 10 mM glucose (pH 7.4). The pipette solution contained 110 mM $BaCl_2$ and 10 mM HEPES (pH 7.4). 750-ms voltage steps were given every 5 s from a V_h of –100 mV. Details of current recordings and analyses, including voltage dependence of inactivation and activation and action potential train, are described in the **Supplementary Methods**.

Suppression of the action of endogenous RIMs using siRNAs and BADN in PC12 cells. The sense siRNA sequences 5′-AAGAATGGACCACAAATGCTT-3′ and 5′-AAGGTGATTGGATGGTATAAA-3′ for rat RIM1, and 5′-AAGGC CCAGATACTCTTAGAT-3′ and 5′-AAGAACTATCCAACATGGTAA-3′ for rat RIM2, were used. Suppression of RNA expression was confirmed by RT-PCR analyses (**Supplementary Fig. 7**). The cells transfected with 8.0 μg pCI-neo-BADN or 8.0 μg pCI-neo-RIM1 were subjected to current recordings 72–96 h after transfection. For details, see the **Supplementary Methods**.

Release assay and RNA analysis in PC12 cells. RNA expression of the α_1 subunits, β subunits, RIM1 or RIM2 in PC12 cells was determined by RT-PCR (**Supplementary Fig. 7**; see **Supplementary Table 9** online for primers). ACh secretion experiments were carried out as previously reported with slight modifications[42]. PC12 cells were plated in poly-D-lysine–coated 35-mm dishes (BD Bioscience) with 5×10^5 cells per dish. Cells were cotransfected with 1 μg of pEFmChAT encoding mouse *Chat* cDNA and RIM1 plasmids at equal molar quantity (3.4 μg of $RIM1_{11–399}$, 3.8 μg of $RIM1_{400–1078}$, 3.4 μg of $RIM1_{1079–1463}$ or 5.0 μg of RIM1) and BADN (10 μg) using Lipofectamine 2000 (Invitrogen). ACh secretion experiments were carried out 3 d after transfection. For details, see the **Supplementary Methods**.

Glutamate release assay using cerebellar neuron primary cultures. Cerebellar granular cells were plated on polyethylenimine-coated 35-mm diameter culture dishes (BD Falcon) at a density of 4.5×10^6–5.0×10^6 cells per dish. BADN or RIM1 cDNAs were introduced with Sindbis viruses in cerebellar neurons. At 24 h after infection, high K^+–evoked glutamate release was carried out. For details, see the **Supplementary Methods**.

Statistical analysis. All data accumulated under each condition from at least three independent experiments are expressed as means ± s.e.m. Student's *t*-test, Kolmogorov-Smirnov test or ANOVA followed by Fisher's test were employed.

Note: Supplementary information is available on the Nature Neuroscience website.

ACKNOWLEDGMENTS

We thank A. Miyawaki for NPY-Venus, R.Y. Tsien for mCherry, S. Ozawa for pSinEGdsp vector, H. Hibino, H Atomi and H. Okuno for helpful discussions, K. Yamazaki, K. Ueda, N. Yokoi and Y. Honjo for expert experiments and K. Sugimoto and T. Morii for molecular modeling. This study was supported by research grants from the Ministry of Education, Culture, Sports, Science and Technology of Japan, the Japan Society for the Promotion of Science and the Human Frontier Science Program. K.P.C. is an Investigator of the Howard Hughes Medical Institute.

AUTHOR CONTRIBUTIONS

S.K., M.W., T.M. and Y.U. contributed to the acquisition, analysis and interpretation of data, and drafting of the manuscript. H.B., A.M.B., M.T. and K.P.C. contributed to the analysis and interpretation of data, and drafting of the manuscript. E.M., Y.H., M.N., M.D.W., M.K. and M.I. contributed to the acquisition, analysis and interpretation of data. Y.M. contributed to the analysis and interpretation of data, and drafting and critical review of the manuscript.

COMPETING INTERESTS STATEMENT

The authors declare no competing financial interests.

Published online at http://www.nature.com/natureneuroscience
Reprints and permissions information is available online at http://npg.nature.com/reprintsandpermissions

1. Zhai, R.G. & Bellen, H.J. The architecture of the active zone in the presynaptic nerve terminal. *Physiology (Bethesda)* **19**, 262–270 (2004).
2. Atwood, H.L. Gatekeeper at the synapse. *Science* **312**, 1008–1009 (2006).
3. Neher, E. Vesicle pools and Ca^{2+} microdomains: new tools for understanding their roles in neurotransmitter release. *Neuron* **20**, 389–399 (1998).
4. Wang, Y., Okamoto, M., Schmitz, F., Hofmann, K. & Südhof, T.C. Rim is a putative Rab3 effector in regulating synaptic-vesicle fusion. *Nature* **388**, 593–598 (1997).
5. Wang, Y. & Südhof, T.C. Genomic definition of RIM proteins: evolutionary amplification of a family of synaptic regulatory proteins. *Genomics* **81**, 126–137 (2003).
6. Wang, Y., Sugita, S. & Südhof, T.C. The RIM/NIM family of neuronal C_2 domain proteins. *J. Biol. Chem.* **275**, 20033–20044 (2000).
7. Betz, A. *et al.* Functional interaction of the active zone proteins Munc13-1 and RIM1 in synaptic vesicle priming. *Neuron* **30**, 183–196 (2001).
8. Ohtsuka, T. *et al.* CAST: a novel protein of the cytomatrix at the active zone of synapses that forms a tenary complex with RIM1 and Munc13-1. *J. Cell Biol.* **158**, 577–590 (2002).
9. Schoch, S. *et al.* RIM1α forms a protein scaffold for regulating neurotransmitter release at the active zone. *Nature* **415**, 321–326 (2002).
10. Coppola, T. *et al.* Direct interaction of the Rab3 effector RIM with Ca^{2+} channels, SNAP-25, and synaptotagmin. *J. Biol. Chem.* **276**, 32756–32762 (2001).
11. Castillo, P.E., Schoch, S., Schmitz, F., Südhof, T.C. & Malenka, R.C. RIM1α is required for presynaptic long-term potentiation. *Nature* **415**, 327–330 (2002).
12. Calakos, N., Schoch, S., Südhof, T.C. & Malenka, R.C. Multiple roles for the active zone protein RIM1α in late stages of neurotransmitter release. *Neuron* **42**, 889–896 (2004).

13. Tsien, R.W., Ellinor, P.T. & Horne, W.A. Molecular diversity of voltage-dependent Ca^{2+} channels. *Trends Pharmacol. Sci.* **12**, 349–354 (1991).
14. Takahashi, T. & Momiyama, A. Different types of calcium channels mediate central synaptic transmission. *Nature* **366**, 156–158 (1993).
15. Wheeler, D.B., Randell, A. & Tsien, R.W. Roles of N-type and Q-type Ca^{2+} channels in supporting hippocampal synaptic transmission. *Science* **264**, 107–111 (1994).
16. Catterall, W.A. Structure and function of neuronal Ca^{2+} channels and their role in neurotransmitter release. *Cell Calcium* **24**, 307–323 (1998).
17. Ertel, E.A. *et al.* Nomenclature of voltage-gated calcium channels. *Neuron* **25**, 533–535 (2000).
18. Sheng, Z-H., Rettig, J., Takahashi, M. & Catterall, W.A. Identification of a syntaxin-binding site of N-type calcium channels. *Neuron* **13**, 1303–1313 (1994).
19. Bezprozvanny, I., Scheller, R.H. & Tsien, R.W. Functional impact of syntaxin on gating of N-type and Q-type calcium channels. *Nature* **378**, 623–626 (1995).
20. Zhong, H., Yokoyama, C.T., Scheuer, T. & Catterall, W.A. Reciprocal regulation of P/Q-type Ca^{2+} channels by SNAP-25, syntaxin and synaptotagmin. *Nat. Neurosci.* **2**, 939–941 (1999).
21. Spafford, J.D. & Zamponi, G.W. Functional interactions between presynaptic calcium channels and the neurotransmitter release machinery. *Curr. Opin. Neurobiol.* **13**, 308–314 (2003).
22. Maximov, A., Südhof, T.C. & Bezprozvanny, I. Association of neuronal calcium channels with modular adaptor proteins. *J. Biol. Chem.* **274**, 24453–24456 (1999).
23. Maximov, A. & Bezprozvany, I. Synaptic targeting of N-type calcium channels in hippocampal neurons. *J. Neurosci.* **22**, 6939–6952 (2002).
24. Nishimune, H., Sanes, J.R. & Carlson, S.S. A synaptic laminin–calcium channel interaction organizes active zones in motor nerve terminals. *Nature* **432**, 580–587 (2004).
25. Kang, M.G. *et al.* A functional AMPA receptor–calcium channel complex in the postsynaptic membrane. *Proc. Natl. Acad. Sci. USA* **103**, 5561–5566 (2006).
26. Mori, Y. *et al.* Primary structure and functional expression from complementary DNA of a brain calcium channel. *Nature* **350**, 398–402 (1991).
27. Bichet, D. *et al.* The I–II loop of the Ca^{2+} channel α_1 subunit contains an endoplasmic reticulum retention signal antagonized by the β subunit. *Neuron* **25**, 177–190 (2000).
28. Varadi, G., Lory, P., Schultz, D., Varadi, M. & Schwartz, A. Acceleration of activation and inactivation by the β subunit of the skeletal muscle calcium channel. *Nature* **352**, 159–162 (1991).
29. Béguin, P. *et al.* Regulation of Ca^{2+} channel expression at the cell surface by the small G-protein kir/Gem. *Nature* **411**, 701–706 (2001).
30. Hibino, H. *et al.* Direct interaction with a nuclear protein and regulation of gene silencing by a variant of the Ca^{2+} channel β_4 subunit. *Proc. Natl. Acad. Sci. USA* **100**, 307–312 (2003).
31. Vendel, A.C. *et al.* Alternative splicing of the voltage-gated Ca^{2+} channel β_4 subunit creates a uniquely folded N-terminal protein binding domain with cell-specific expression in the cerebellar cortex. *J. Neurosci.* **26**, 2635–2644 (2006).
32. Burgess, D.L. *et al.* β subunit reshuffling modifies N- and P/Q-type Ca^{2+} channel subunit compositions in *lethargic* mouse brain. *Mol. Cell. Neurosci.* **13**, 293–311 (1999).
33. Opatowsky, Y., Chen, C.C., Campbell, K.P. & Hirsch, J.A. Structural analysis of the voltage-dependent calcium channel β-subunit functional core and its complex with the α_1 interaction domain. *Neuron* **42**, 387–399 (2004).
34. Khanna, R., Li, Q., Sun, L., Collins, T.J. & Stanley, E.F. N-type Ca^{2+} channels and RIM scaffold protein covary at the presynaptic transmitter release face, but are components of independent protein complexes. *Neuroscience* **140**, 1201–1208 (2006).
35. Plummer, M.R., Logothetis, D.E. & Hess, P. Elementary properties and pharmacological sensitivities of calcium channels in mammalian peripheral neurons. *Neuron* **2**, 1453–1463 (1989).
36. Patil, P.G., Brody, D.L. & Yue, D.T. Preferential closed-state inactivation of neuronal calcium channels. *Neuron* **20**, 1027–1038 (1998).
37. De Waard, M., Pragnell, M. & Campbell, K.P. Ca^{2+} channel regulation by a conserved β-subunit domain. *Neuron* **13**, 495–503 (1994).
38. DeMaria, C.D., Soong, T.W., Alseikhan, B.A., Alvania, R.S. & Yue, D.T. Calmodulin bifurcates the local Ca^{2+} signal that modulates P/Q-type Ca^{2+} channels. *Nature* **411**, 484–489 (2001).
39. Stanley, E.F. Syntaxin I modulation of presynaptic calcium channel inactivation revealed by botulinum toxin C1. *Eur. J. Neurosci.* **17**, 1303–1305 (2003).
40. Dulubova, I. *et al.* A Munc13/RIM/Rab3 tripartite complex: from priming to plasticity? *EMBO J.* **24**, 2839–2850 (2005).
41. Liu, H. *et al.* Expression and subunit interaction of voltage-dependent Ca^{2+} channels in PC12 cells. *J. Neurosci.* **16**, 7557–7565 (1996).
42. Nishiki, T. *et al.* Comparison of exocytotic mechanisms between acetylcholine- and catecholamine-containing vesicles in rat pheochromocytoma cells. *Biochem. Biophys. Res. Commun.* **239**, 57–62 (1997).
43. Zhang, J.F., Ellinor, P.T., Aldrich, R.W. & Tsien, R.W. Molecular determinants of voltage-dependent inactivation in calcium channels. *Nature* **372**, 97–100 (1994).
44. Stotz, S.C., Hamid, J., Spaetgens, R.L., Jarvis, S.E. & Zamponi, G.W. Fast inactivation of voltage-dependent calcium channels. *J. Biol. Chem.* **275**, 24575–24582 (2000).
45. Geib, S. *et al.* The interaction between the I–II loop and the III–IV loop of $Ca_v2.1$ contributes to voltage-dependent inactivation in a β-dependent manner. *J. Biol. Chem.* **277**, 10003–10013 (2002).
46. Weimer, R.M. *et al.* UNC-13 and UNC-10/Rim localize synaptic vesicles to specific membrane domains. *J. Neurosci.* **26**, 8040–8047 (2006).
47. Schoch, S. *et al.* Redundant functions of RIM1α and RIM2α in Ca^{2+}-triggered neurotransmitter release. *EMBO J.* **25**, 5852–5863 (2006).
48. Hibino, H. *et al.* RIM-binding proteins (RBPs) couple Rab3-interacting molecules (RIMs) to voltage-gated Ca^{2+} channels. *Neuron* **34**, 411–423 (2002).
49. Koushika, S.P. *et al.* A post-docking role for active zone protein Rim. *Nat. Neurosci.* **4**, 997–1005 (2001).
50. Nonaka, M., Doi, T., Fujiyoshi, Y., Takemoto-Kimura, S. & Bito, H. Essential contribution of the ligand-binding βB/βC loop of PDZ1 and PDZ2 in the regulation of postsynaptic clustering, scaffolding and localization of postsynaptic density-95. *J. Neurosci.* **26**, 763–774 (2006).

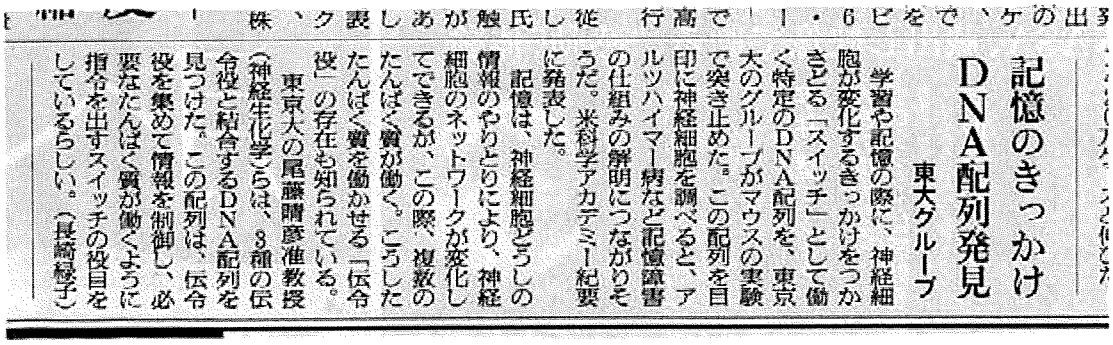

記憶のきっかけ DNA配列発見

東大グループ

学習や記憶の際に、神経細胞が変化するきっかけをつくる「スイッチ」として働く特定のDNA配列を、東京大のグループがマウスの実験で突き止めた。この配列を目印に神経細胞を調べると、アルツハイマー病など記憶障害の仕組みの解明につながりそうだ。米科学アカデミー紀要に発表した。

記憶は、神経細胞どうしの情報のやりとりにより、神経細胞のネットワークが変化してできるが、この際、複数のたんぱく質が働く。こうしたたんぱく質を働かせる「伝令役」の存在も知られている。

東京大の尾藤晴彦准教授(神経生化学)らは、3種の伝令役と結合するDNA配列を見つけた。この配列は、伝令役を集めて情報を制御し、必要なたんぱく質が働くように指令を出すスイッチの役目をしているらしい。(長崎緑子)

朝日新聞
2009年1月15日　夕刊9面掲載

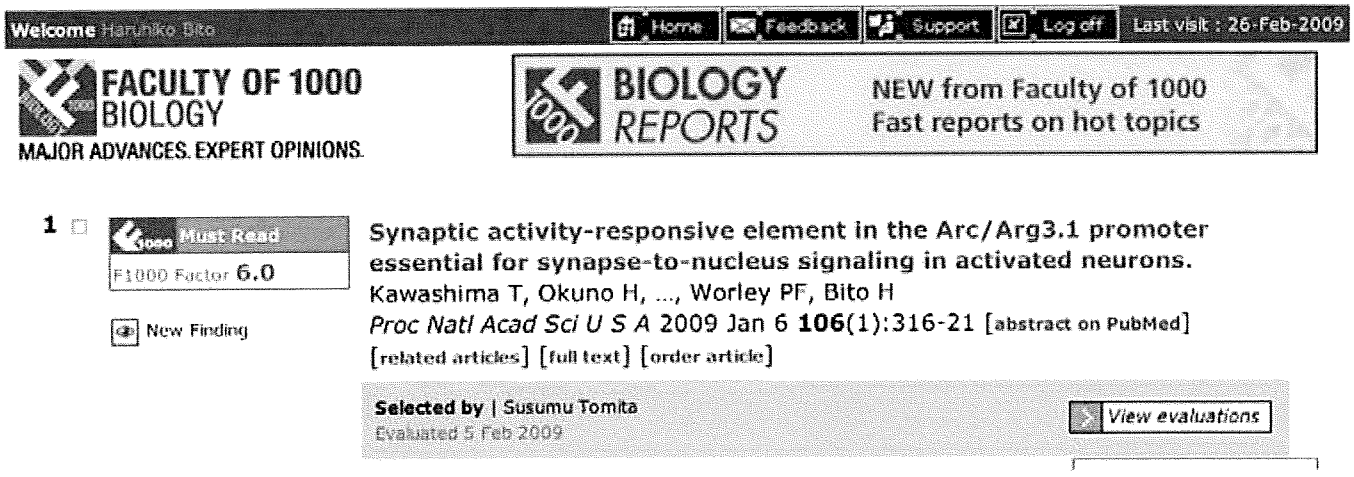

最も権威ある論文ピアレビューサイトであるF1000 Biologyにて Must Read(必読)論文として2009年2月5日付けで紹介

Synaptic activity-responsive element in the *Arc/Arg3.1* promoter essential for synapse-to-nucleus signaling in activated neurons

Takashi Kawashima[a,1], Hiroyuki Okuno[a,1,2], Mio Nonaka[a], Aki Adachi-Morishima[a], Nan Kyo[a], Michiko Okamura[a], Sayaka Takemoto-Kimura[a], Paul F. Worley[b], and Haruhiko Bito[a,c,2]

[a]Department of Neurochemistry, Graduate School of Medicine, University of Tokyo, Bunkyo-ku, Tokyo 113-0033, Japan; [c]CREST-JST, Kawaguchi, Saitama 332-0012, Japan; and [b]Department of Neuroscience, Johns Hopkins University School of Medicine, Baltimore, MD 21205

Edited by Yoshito Kaziro, Kyoto University, Kyoto, Japan, and approved November 17, 2008 (received for review July 14, 2008)

The neuronal immediate early gene *Arc/Arg-3.1* is widely used as one of the most reliable molecular markers for intense synaptic activity in vivo. However, the *cis*-acting elements responsible for such stringent activity dependence have not been firmly identified. Here we combined luciferase reporter assays in cultured cortical neurons and comparative genome mapping to identify the critical synaptic activity-responsive elements (SARE) of the *Arc/Arg-3.1* gene. A major SARE was found as a unique ≈100-bp element located at >5 kb upstream of the *Arc/Arg-3.1* transcription initiation site in the mouse genome. This single element, when positioned immediately upstream of a minimal promoter, was necessary and sufficient to replicate crucial properties of endogenous *Arc/Arg-3.1*'s transcriptional regulation, including rapid onset of transcription triggered by synaptic activity and low basal expression during synaptic inactivity. We identified the major determinants of SARE as a unique cluster of neuronal activity-dependent *cis*-regulatory elements consisting of closely localized binding sites for CREB, MEF2, and SRF. Consistently, a SARE reporter could readily trace and mark an ensemble of cells that have experienced intense activity in the recent past in vivo. Taken together, our work uncovers a novel transcriptional mechanism by which a critical 100-bp element, SARE, mediates a predominant component of the synapse-to-nucleus signaling in ensembles of Arc/Arg-3.1-positive activated neurons.

immediate-early genes | MEF2 | SRF | calcium | CREB

Fine tuning of gene expression and protein translation in mature neurons is of vital importance to brain function (1). Aberrance of adaptive responses such as long-term memory or late-phase synaptic plasticity has indeed been the hallmark of several genetically engineered mouse mutants in which the expression or the function of key transcription factors have been altered (2, 3). Thus it appears that the supply of neuronal proteins must be tightly matched to the cellular demand at any given time, to maintain proper neuronal circuit function.

One critical determinant of neuronal gene expression is the neuron's own activity. Dramatic changes in gene expression have been reported upon robust reorganization of sensory information processing (such as during critical period plasticity of the visual cortex), or through characteristic cognitive processes (such as establishment of long-term memory) (4–6). Barrages of synaptic activity that alters synaptic strength can directly up- or downregulate various constituents of the synaptic machinery and many signaling molecules (7–9). Studies of the transcriptional activation mechanisms leading to upregulation of the immediate early genes c-*fos*, *zif*268, and of the brain-derived neurotrophic factor (BDNF) indicated that transcription factors such as the Ca^{2+}/cAMP-response element binding protein (CREB) and the serum response factor (SRF) may play a privileged role as key neuronal activity sensors in the nucleus (10–12).

An activity-regulated cytoskeleton-associated protein (Arc/Arg-3.1) has recently emerged as an attractive candidate effector molecule/immediate early gene product (13, 14), whose induction may correlate, at least in part, with the induced synaptic alteration phenotype (15–18). Furthermore, *Arc/Arg-3.1* transcription is induced extremely rapidly and *Arc/Arg-3.1* mRNA detection, by fluorescence in situ hybridization, has now been validated as a reliable trace of intense synaptic activity within a neuronal ensemble in the hippocampus (e.g., during novelty exposure), in the amygdala (e.g., during acquisition of long-term fear memory), or in the sensory cortices (e.g., after intense sensory experience following sensory deprivation) (19–22). Despite the growing interest in Arc/Arg-3.1 function, however, surprisingly little is yet known about the genomic mechanism by which acute delivery of synaptic information can be reliably encoded into *Arc/Arg-3.1* transcriptional events in the nucleus. To address this question, we investigated the *cis*-acting enhancer elements responsible for such stringent neuronal activity dependence.

Results

Presence of a Strong Synaptic Activity-Responsive Element in a Distal Portion of the Mouse *Arc/Arg-3.1* Promoter. We performed transcriptional reporter assays using primary culture neurons in which endogenous *Arc/Arg-3.1* is rapidly and transiently induced by 4AP/BIC stimulation (Fig. 1*A*). In the mouse genome, 7 conserved regions exceeding 65% identity per 100 bp with humans were found between 0 and −5 kb (from the transcription initiation site), and 1 distal region was mapped between −6 kb and −7 kb (Fig. 1*B*). No further conserved regions were found between −7 kb and −10 kb.

Prior studies have demonstrated the role of a proximal region (<2 kb) of the *Arc/Arg-3.1* promoter in its activity dependence (23, 24). Consistent with this, proximal regions [Arc1000 (−996 to +198) and Arc2000 (−1996 to +198)] showed 2- to 3-fold induction after stimulation in our assays (Fig. 1*C*). Genomic regions up to 3 kb (Arc3000, −2996 to +198) conferred an 8-fold induction (Fig. 1*C*). The activated levels of 4-kb and 5-kb fragments [Arc4000 (−3996 to +198) and Arc5000 (−4996 to +198)] were similar to that of Arc3000, but their basal levels in TTX were significantly lower than those of Arc1000, Arc2000, and Arc3000 ($P < 0.01$), resulting in an ≈20-fold induction (Fig. 1*C*). Unexpectedly, extension of the genomic sequence up to 7 kb (Arc7000, −7065 to +198) resulted in further increase in its induction ability, of >150-fold, in

Author contributions: H.O. and H.B. designed research; T.K., H.O., M.N., and N.K. performed research; A.A.-M., M.O., S.T.-K., and P.F.W. contributed new reagents/analytic tools; T.K., H.O., M.N., N.K., and H.B. analyzed data; and T.K., H.O., M.N., and H.B. wrote the paper.

The authors declare no conflict of interest.

This article is a PNAS Direct Submission.

[1]T.K. and H.O. contributed equally to this work.

[2]To whom correspondence may be addressed. E-mail: hbito@m.u-tokyo.ac.jp or okuno@m.u-tokyo.ac.jp.

This article contains supporting information online at www.pnas.org/cgi/content/full/0806518106/DCSupplemental.

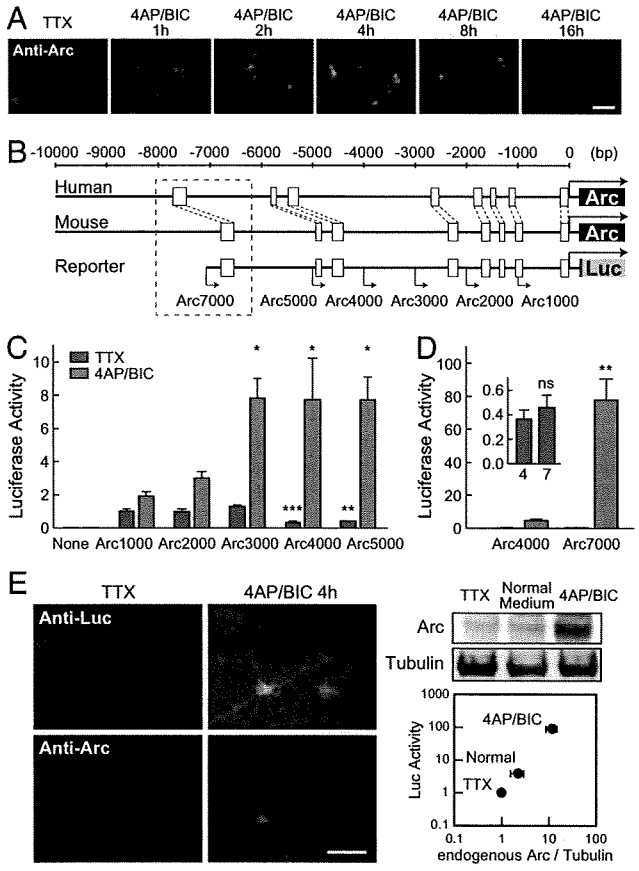

Fig. 1. Multiple regulatory elements in the mouse *Arc/Arg-3.1* promoter. (*A*) Time course of endogenous Arc/Arg-3.1 protein induction by 4AP/BIC stimulation. Cultured cortical neurons pretreated with TTX were stimulated with 4AP/BIC for indicated hours. (Scale bar, 100 μm.) (*B*) Evolutionarily conserved genomic regions in the upstream of the *Arc/Arg-3.1* gene. Regions conserved between mice and humans are shown as white boxes. A destabilized luciferase (Luc-PEST) gene was used as a reporter. (*C*) Transcriptional regulatory activities of Arc1000–5000. Cultured cortical neurons were stimulated with 4AP/BIC for 4 h. Luciferase activities are normalized relative to the activity of Arc1000 under the TTX treatment. This normalization applies to all luciferase assay data in this study. Statistical analyses were performed separately for the TTX and 4AP/BIC data sets. n = 5 independent experiments. *, $P < 0.05$; **, $P < 0.01$; ***, $P < 0.001$ compared with the TTX or the 4AP/BIC value of Arc1000 (1-way ANOVA with Tukey's test). (*D*) Strong activation ability of Arc7000. The y axis for the basal levels were expanded and shown in the inset for clarity. n = 7 independent experiments. **, $P < 0.01$; ns, not significant (paired t test) compared with the 4AP/BIC or the TTX value of Arc4000. (*E*) Arc7000-driven luciferase correlates with endogenous Arc induction. *Left*, coexpression of luciferase and endogenous Arc protein after stimulation. (Scale bar, 50 μm.) *Right*, simultaneous quantification of luciferase activities and endogenous Arc protein levels in the same samples. Cell lysates were prepared from neurons with no treatment (normal medium), with TTX, or with 4AP/BIC for 4 h. Arc protein levels were quantified by Western blotting and plotted against the reporter luciferase activities. Duplicated samples were analyzed and shown.

response to stimulation ($P < 0.01$) (Fig. 1*D*), indicating the presence of a very potent enhancer in the most distal conserved region.

We also examined the relative potency of Arc7000 at single-cell resolution, using a destabilized GFP as a fluorescent reporter. As expected from the results of luciferase assays, GFP signals in individual neurons were more elevated downstream of Arc7000 than of Arc4000 ($P < 0.001$) [supporting information (*SI*) Fig. S1]. Additionally, no GFP signals were detected in glial cells (data not shown), indicating that Arc7000 may also determine the neuron-specific expression pattern of the *Arc/Arg-3.1* gene.

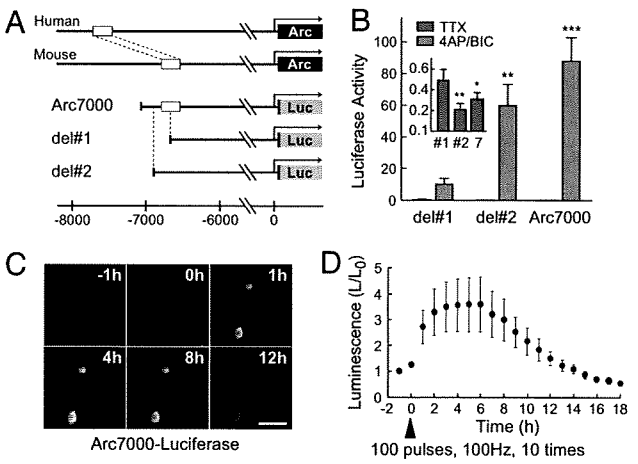

Fig. 2. The distal conserved region is crucial for the Arc7000 promoter activity. (*A*) Arc7000 deletion mutants. The genomic locus framed by a dashed box in Fig. 1 *B* is expanded and shown. (*B*) Presence of a potent enhancer element between Arc7000-del no. 1 and Arc7000-del no. 2. n = 6 independent experiments. *, $P < 0.05$; **, $P < 0.01$; ***, $P < 0.001$, compared with the TTX or the 4AP/BIC value of Arc7000-del no. 1 (1-way ANOVA with Tukey's test). (*C* and *D*) Rapid and transient induction of luciferase luminescence by Arc7000 after high-frequency electrical stimulation. Hippocampal neurons transfected with a click beetle luciferase (ELuc) vector was electrically stimulated at 0 h (triangle), and luminescence in the soma was monitored. Representative images were shown in *C*. n = 9 neurons. (Scale bar, 50 μm.)

The Arc7000 activity correlated well with the endogenous *Arc/Arg-3.1* expression, because the reporter luciferase after stimulation was mostly coexpressed in the same cells as endogenously induced Arc/Arg-3.1 (Fig. 1*E*), and Western blots showed a linear relation between luciferase activity and endogenous Arc protein levels (Fig. 1*E*).

Identification of a Synaptic Activity-Responsive Element (SARE) in Arc7000 That Is Critical for Activity-Regulated Gene Expression. To pin down the critical enhancer element, we next examined a genomic deletion (del) mutant Arc7000-del no. 1 (−6667 to +198), in which the most distal conserved region was truncated (Fig. 2*A*). This mutant revealed a striking decrease in activity dependence compared with Arc7000 ($P < 0.01$) (Fig. 2*B*). In contrast, Arc7000-del no. 2 (−6893 to +198), in which the conserved region was spared, possessed an activity dependence indistinguishable from Arc7000 (Fig. 2 *A* and *B*). Intriguingly, the basal level of Arc7000-del no. 2 in TTX was indistinguishable from that of Arc7000, but was significantly lower than that of Arc7000-del no. 1 ($P < 0.05$) (Fig. 2*B*).

We then tested whether robust high-frequency synaptic activity triggered by electrical stimulation could induce reporter gene expression downstream of Arc7000 in single neurons. Hippocampal neurons transfected with an Arc7000-ELuc-PEST plasmid were stimulated with field electrical pulses. In responding neurons, luminescence started to increase immediately after the stimulation, reached plateau after 4–6 h, and attenuated gradually after 8 h (Fig. 2 *C* and *D*). This activation time course closely resembled the induction time course of endogenous *Arc/Arg-3.1* following electrical stimulation in vivo (25).

These findings were most consistent with the presence of a potent enhancer, which we termed SARE, in a region between Arc7000-del no. 1 and Arc7000-del no. 2 (Fig. 2 *A* and *B*). Close examination of the evolutionarily conserved region present in del no. 2 but truncated in del no. 1 revealed a series of short conserved sequence stretches, of ≈100 bp (Fig. 3*A*).

To directly test the role of these sequence stretches, we fused a 104-bp fragment (−6793 to −6690) to a TATA-containing short

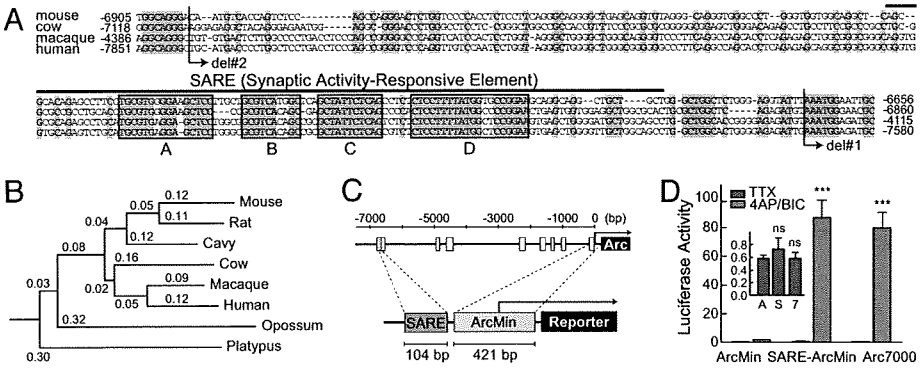

Fig. 3. *Arc/Arg-3.1* SARE replicates Arc7000 promoter activity. (*A*) Comparison across multiple mammalian species. Conserved sequences were highlighted in gray. A short stretch of sequences (thick line) consisted of 4 highly conserved boxes (boxes *A–D*) was termed a synaptic activity responsive element (SARE). (*B*) Dendrogram showing the divergence of SARE sequences across various mammalian species. The numbers represent the branch length, which indicates the degree of nucleotide differences. Detailed nucleotide information for this analysis is shown in Fig. S3. (*C*) SARE-ArcMin reporter vector. SARE was fused directly upstream of ArcMin, a TATA-containing sequence around the transcription initiation site of the *Arc/Arg-3.1* gene. (*D*) SARE-ArcMin replicates the activation ability of Arc7000. $n = 5$ independent experiments. ***, $P < 0.001$; ns, not significant, compared with the TTX or the 4AP/BIC value of ArcMin (1-way ANOVA with Tukey's test).

promoter (−222 to +198) of the *Arc/Arg-3.1* gene (SARE-ArcMin) (Fig. 3 *A* and *C*). Luciferase activity driven by SARE-ArcMin was increased >100-fold in response to stimulation (Fig. 3*D*). The basal levels did not differ between SARE-ArcMin and ArcMin (Fig. 3*D*). Importantly, the activation level of SARE-ArcMin was indistinguishable from that of Arc7000 (Fig. 3*D*). The fluorescent protein reporter assay also revealed a dramatic increase in GFP signal positivity in SARE-ArcMin reporter-transfected neurons, following synaptic stimulation in individual cells (Fig. S2). None of the other conserved genomic regions showed such strong enhancer activities on their own (data not shown).

Taken together, these results indicate the existence of a novel SARE in the distal *Arc/Arg-3.1* promoter, which appeared to be critical for replicating the amplitude of activity-induced transcriptional response of the full promoter in the absence of any other adjacent genomic regions, when placed immediately upstream of the minimal *Arc/Arg-3.1* promoter.

Contribution of 3 Activity-Regulated Transcription Factors, CREB, MEF2, and SRF, in SARE Activation. SARE contained 4 conserved sequence stretches (Fig. 3*A*). This raised the possibility that perhaps distinct transcription factors could in principle bind to SARE, and thus, these putative binding sites were tentatively called boxes *A*−*D* (Fig. 3*A*). All 4 boxes were conserved in most mammals, except some species such as the opossum and the platypus (Fig. 3*B* and Fig. S3). To address their requirements, we introduced mutations in each of these boxes, and tested them either in the upstream of a TATA-containing minimal CMV promoter (minCMV, which has virtually no transcriptional activity per se), or in the context of the full Arc7000 promoter (Fig. 4 *A* and *B*). Luciferase activity of SARE-minCMV was increased >80-fold in response to stimulation, and this induction was dramatically diminished by single mutations in boxes *B*, *C*, and *D* ($P < 0.001$). In contrast, a mutation in box *A* had no significant effect (Fig. 4*A*). Combined mutations in both boxes *B* and *D* almost completely blocked the induction (Fig. 4*A*). Similar results were obtained in the context of the full Arc7000 promoter (Fig. 4*B*). These data suggested that boxes *B*, *C*, and *D* were required for the enhancer activity of SARE, and some cooperativity might exist between them. Additionally, the basal level of SARE-minCMV was significantly elevated by mutating box *D* ($P < 0.001$) (Fig. 4*A*), indicating that box *D* might also contribute to attenuating transcription during synaptic inactivity.

We next sought to identify the transcription factors that bound to these sites. Box *B* contained a sequence matching a half site of the consensus binding sequence for CREB (Fig. 4*C*). Box *C* matched the consensus for myocyte enhancer factor 2 (MEF2) with the exception of 2 nucleotides (Fig. 4*C*). The 5′-end of box *D* perfectly matched the consensus for SRF, while the 3′-end perfectly matched the consensus for the ternary complex factors (TCFs), the well-characterized accessory proteins of SRF (Fig. 4*C*). An electrophoretic mobility-shift assay (EMSA) revealed the formation of each specific protein-DNA complex for boxes *B*, *C*, and *D* in nuclear extracts obtained from electroconvulsive shock-treated rat cortices (Fig. 4*C*). Consistent with the consensus sequence matches, each complex was disrupted by adding excess amounts of competitor DNA, and gel supershifts were detected using CREB-, MEF2-, and SRF-specific antibodies. Furthermore, chromatin immunoprecipitation (ChIP) assay using neuronal culture confirmed physical binding of CREB, MEF2, and SRF to SARE in cultured neurons (Fig. 4*D* and Fig. S4). Together, these data strongly suggest that CREB, MEF2, and SRF play critical roles in SARE activation via binding to boxes *B*, *C*, and *D*, respectively (Fig. 4*C*).

We further investigated the intracellular signaling pathways upstream of these transcription factors. The SARE activation in the context of Arc7000 by 4AP/BIC treatment was almost completely suppressed when both AMPA-R and NMDA-R were blocked, confirming that excitatory synaptic inputs trigger the activation (Fig. S5*A*). In addition, the activation was reduced 80% when only NMDA-R was blocked, indicating that synaptic Ca^{2+} influx through NMDA-R is critical for the SARE activation (Fig. S5*A*). The activation was also significantly diminished by KN-93, a Ca^{2+}/calmodulin-dependent protein kinase (CaMK) inhibitor, and U0126, a mitogen-activated protein kinase kinase (MEK) inhibitor (Fig. S5*B*). An essentially similar pharmacological profile was obtained when the SARE activity was tested in the upstream of the minimal CMV promoter (Fig. S5*C*). These results confirmed that SARE was crucial for a large part of the transcriptional response of the *Arc/Arg-3.1* gene that lied downstream of activity-regulated signaling mechanisms, such as CaMK and MAPK cascades, both of which were previously shown to underlie many aspects of neuronal adaptive responses (8, 26).

Visualization of Activated Cells in a Neuronal Circuit Using a SARE Reporter Lentivirus Vector. One potential caveat of the above experiments was that these in vitro assays did not involve genomic integration of the reporter genes. Therefore, we designed a lentivirus-based gene delivery system to introduce SARE-driven reporters into the neuronal genome (Fig. 5). We constructed a lentivirus vector containing 2 expression cassettes placed in opposite directions and separated by an insulator sequence. In 1 cassette,

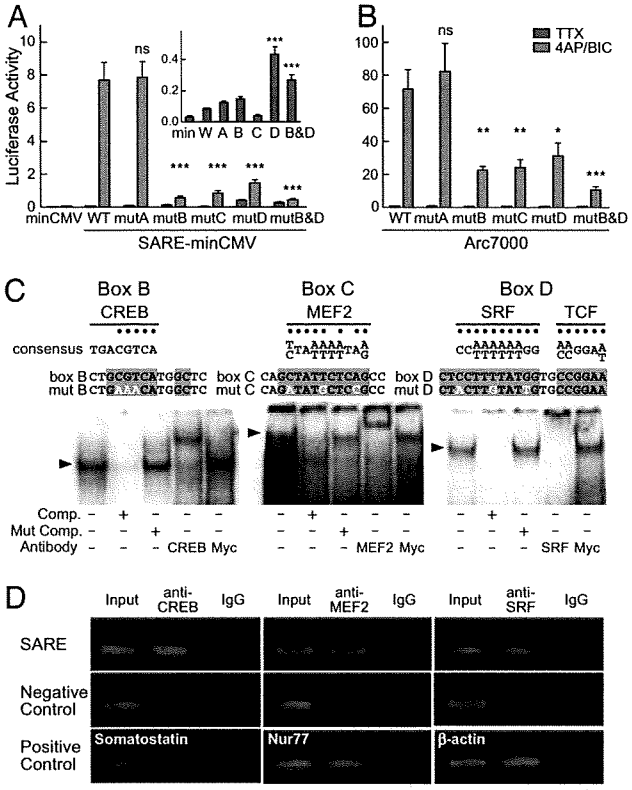

Fig. 4. Involvement of coclustered CREB, MEF2, and SRF in the SARE activation. (*A*) Loss of the SARE activity by mutations in the boxes *B*, *C*, and *D*, but not *A*, in the context of a minimal CMV promoter (SARE-minCMV). Note that the basal level (TTX) was elevated by a mutation in the box *D* (inset). WT, wild-type; ***, $P < 0.001$; ns, not significant, compared with the TTX or the 4AP/BIC value of WT (1-way ANOVA with Tukey's test). (*B*) Loss of the Arc7000 activity by mutations in the boxes *B*, *C*, and *D*. WT, wild-type; *, $P < 0.05$; **, $P < 0.01$; ***, $P < 0.001$; ns, not significant, compared with the 4AP/BIC value of WT (1-way ANOVA with Tukey's test). (*C*) EMSA revealed binding of CREB, MEF2, and SRF to the boxes *B*, *C*, and *D*. *Top*, the matched nucleotides are indicated by dots. The evolutionarily conserved nucleotides are highlighted in gray. The mutated nucleotides are shown with white letters. *Bottom*, representative results of EMSA. The brain nuclear extracts were added with probes of the boxes *B*, *C*, and *D*. Specific DNA-protein complexes (arrows) were observed, which disappeared by adding excessive amounts of unlabeled competitors (Comp), but not by mutated competitors (Mut Comp). Antibodies against CREB, MEF2, and SRF disrupted or supershifted the complexes, whereas a control antibody (anti-Myc) had no effects. (*D*) Chromatin immunoprecipitation (ChIP) assays revealed physical binding of CREB, MEF2, and SRF to SARE in the genome. Target genomic sequences were amplified with specific primer sets by qPCR. *Left*, the genomic region adjacent to the SARE sequence (within 200 bp) was detected in the immunoprecipitates obtained using an anti-CREB antibody, while a negative control sequence 10 kb downstream of SARE was not. The Somatostatin promoter was used as a positive control. *Middle*, detection of SARE in the immunoprecipitates obtained using an anti-MEF2 antibody. The Nur77 promoter was used as a positive control. *Right*, detection of SARE in the immunoprecipitates obtained using an anti-SRF antibody. The β-actin promoter was used as a positive control.

an RFP marker (TurboFP635) was driven under the control of a constitutive *pgk* promoter, while in the other, a d2EGFP reporter was expressed under the control of SARE-ArcMin. A control virus vector contained all these elements except for SARE (Fig. 5*A*).

BDNF is known to effectively induce endogenous Arc/Arg-3.1 expression in neurons. When SARE-ArcMin lentivirus-infected neurons were stimulated with BDNF, GFP signals became detectable in individual neurons (Fig. 5*B*). We further examined, by time-lapse live-cell fluorescence imaging, the activation time course of the genome-integrated SARE, upon high-frequency electrical

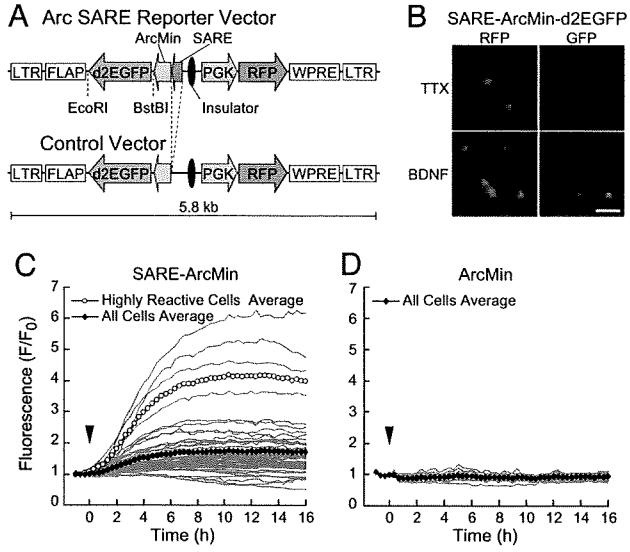

Fig. 5. Lentivirus-based genomic integration of the SARE reporter. (*A*) Design of lentiviral vectors. *Top*, the SARE reporter vector encodes an inducible reporter GFP (d2EGFP) under the control of SARE-ArcMin and a constitutively expressed infection marker RFP (TurboFP635) under the control of a *pgk* promoter. *Bottom*, a control vector lacking SARE. (*B*) Hippocampal neurons infected with the SARE reporter lentivirus were stimulated with BDNF for 6 h at 14 days postinfection. (Scale bar, 50 μm.) (*C*) GFP live-cell imaging of SARE-virus-infected neurons stimulated with high-frequency electrical pulses. Hippocampal neurons infected with the SARE reporter lentivirus were stimulated with field electrical pulses at time 0 h (triangle, 100 pulses at 100 Hz, 9 times), and GFP fluorescence was monitored. Gray lines, traces of individual neurons. Filled squares, the average trace of all neurons examined ($n = 59$). Open circles, the average trace of highly reactive neurons (top 10% of all neurons sorted by the F/F_0 value at the time of 8 h, $n = 6$). (*D*) No GFP fluorescence changes were observed in control-virus-infected neurons. Filled squares, the average trace of all neurons examined ($n = 18$).

stimulation (9 bursts of 100 Hz, 1 sec applied by field stimulation). In most of the SARE-ArcMin lentivirus-infected neurons, GFP fluorescence consistently increased immediately after the stimulation and started to saturate at ≈6–8 h (Fig. 5*C*), while the control virus-infected neurons showed virtually no GFP responses (Fig. 5*D*). Some of the neurons were particularly responsive (Fig. 5*C*), indicative of high copy number expression from multiple and/or transcriptionally favorable genomic loci. Alternatively, these neurons might have been favored because of their highly excitable properties within the neuronal network in culture as previously reported (10).

The above results suggested that the SARE-ArcMin lentivirus might provide a way to visualize specific sets of activated neurons in a given neural circuit in the brain. As a model, we designed an in vivo SARE-ArcMin reporter assay by directly injecting into mouse brains a d2EGFP reporter lentivirus. Consistent with prior reports (27), viral injection into the lateral ventricles of E15 mouse embryos reproducibly resulted in selective integration of infected neurons into layers 2/3 throughout the neocortex, as identified by RFP fluorescence and morphological criteria. No systematic differences were observed in the numbers of infected neurons between the 2 hemispheres. In our conditions, the infection rate was ranging 2–5% of the total cells in layers 2/3.

Cortical activity in the primary visual cortex (V1) was then stimulated by direct manipulation of the visual sensory inputs. Virus-infected mice (3–4 week-old) were sensory-deprived on 1 eye by suture, dark-reared for 1–3 days, and the intact open eye was exposed to light (Fig. 6*A*). Such sensory manipulation produced unilateral activation of the V1, as visualized by high immunoreactivities of endogenous Arc/Arg-3.1 at layers 2/3 and 4 in the

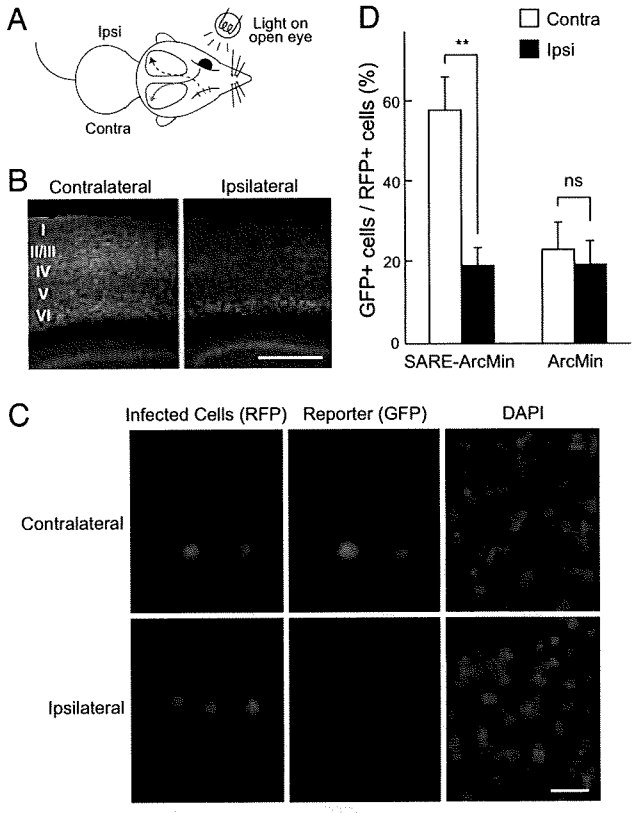

Fig. 6. Visualization of activated neurons in vivo by the SARE viral vector. (*A*) Manipulation of neuronal activity in the mouse visual cortex. The virus-infected mice were sensory-deprived on 1 eye by suture, dark reared for 2–3 days, and exposed to light on the intact open eye. (*B*) Endogenous Arc/Arg-3.1 immunohistochemistry showing unilateral activation of the visual cortex. (Scale bar, 0.5 mm.) (*C*) The SARE reporter virus-infected neurons in layers 2/3 of the visual cortex. Activity-reporter GFP signals were detected in the contralateral side, but not in the ipsilateral side. (Scale bar, 20 μm.) (*D*) The percentages of GFP-positive neurons over RFP-positive neurons in each hemisphere. $n = 6$ mice for SARE-ArcMin, $n = 5$ mice for ArcMin. **, $P < 0.01$; ns, not significant, compared to the ipsilateral side (paired t test).

contralateral, but not in the ipsilateral, visual cortex (Fig. 6*B*) (21). Consistent with this pattern, we found that the majority (58.3 ± 7.9%) of RFP-positive neurons were GFP-positive in the contralateral hemisphere that received visual inputs, whereas only a small number (19.3 ± 4.4%) of neurons were positive in the ipsilateral hemisphere (Fig. 6 *C* and *D*). The percentage of GFP- and RFP-double positive neurons in the contralateral hemisphere were comparable with that of Arc/Arg-3.1- and RFP-double positive neurons (57.8 ± 4.6%) (Fig. S6), consistent with coexpression of reporter GFP and endogenous Arc/Arg-3.1. The control ArcMin virus-infected neurons showed low GFP positivity (about 20%) and did not show imbalances between hemispheres (Fig. 6*D*). Taken together, these results indicate that SARE-ArcMin lentivirus could reliably mark activated neurons within a targeted neuronal circuit.

Discussion

Elucidation of a Novel Transcriptional Switch Mechanism That Links Synaptic Activity with Nuclear Transcription: Participation of 3 Major Activity-Regulated Transcription Factors CREB, SRF, and MEF2 in *Arc/Arg-3.1* Transcriptional Response. Our work indicates that the Arc7000 promoter essentially replicates the transcriptional profile of endogenous *Arc/Arg-3.1*, and that a relatively short DNA sequence of ≈100 bp provides a key regulatory mechanism for synapse-to-nucleus signaling. This novel *cis*-acting element contains binding sites for 3 major activity-dependent transcription factors, CREB, MEF2, and SRF, and drove as much reporter induction as Arc7000, in response to synaptic stimuli, when placed upstream of the *Arc/Arg-3.1* minimal promoter. Mutations in either one of the binding sequences resulted in a severe block of transcriptional activity. Thus, intact promoter occupancy by all 3 factors appears to be essential for proper transcriptional activation upon synaptic activity. Pharmacological analyses revealed that synaptic Ca^{2+} influx through NMDA-R was critical for its activation. On the basis of these findings, we named this main activity-sensor for *Arc/Arg-3.1* transcription "synaptic activity-responsive element (SARE)."

A functional CRE is present on many activity-regulated neuronal genes, and CREB has repeatedly been demonstrated to be a critical factor in establishment of long-term plasticity and long-term memory (1, 2, 20). Similarly, a critical role for SRE and SRF in activity-dependent gene expression has extensively been documented (3). Recent evidence also supports a role for MEF2 upstream of various activity-induced genes which directly regulate synaptic functions (28). However, the discovery of a physical clustering, corequirement and sufficiency of the 3 activity-dependent *cis*-regulatory elements located in such close proximity (≈100 bp) in SARE is particularly striking, suggesting that SARE may have a unique role as a coincidence detector for the 3 activity-dependent transcription factors. Intriguingly, we observed that mutations in the SRF-binding site not only abolished SARE activation, but also significantly augmented basal activity under silenced conditions, suggesting an additional role of SRF for transcriptional repression as previously reported in certain contexts in nonneuronal cells (29).

Although distally located SARE likely acts as a major element for activity-dependent *Arc/Arg-3.1* induction, other proximal elements may further cooperate with SARE. Our own data suggested that a proximal region possessed a 2- to 3-fold transcriptional activation ability, consistent with a previous study that showed the contribution of cAMP/MAPK pathways in the activity-dependent response mediated by this region (23). Furthermore, *Egr-1/3* may also mediate the late, protein-synthesis dependent phase of *Arc/Arg-3.1* induction via binding to this proximal region (24).

Mapping of Active Ensembles Within a Neuronal Circuit Can Be Achieved Using SARE-Based Reporters. Detailed analyses of *Arc/Arg-3.1* expression using in situ hybridization have revealed that *Arc/Arg-3.1* transcription is specifically triggered by task- or sensory input-related information processing in several brain areas, including the hippocampus, amygdala, and cerebral cortex (19–21). The shortness of SARE sequence allows designing a virus-based tool to monitor *Arc/Arg-3.1* expression for both in vitro and in vivo imaging. We here performed an experiment where we injected a SARE-reporter lentivirus into embryonic mouse cerebral ventricles in utero, at embryonic day 15 (E15). Prior work established that only the neuronal progenitor cells, present in the ventricular zone (VZ) on the day of injection, are susceptible to viral infection. VZ cells at E15 are destined to become layers 2/3 neurons in the cerebral cortex (27). More than 20 days after lentiviral infection, when the viral integration into the genome has been completed, we quantified the extent of visual activation in layers 2/3 of the primary visual cortex. The virus-injected mice were first dark reared for more than 24 h, which suppressed the reporter expression to the baseline. Following light exposure to 1 eye for 2–3 h, we found that ≈60% of the infected neurons of layers 2/3 were GFP reporter positive, which is consistent with prior functional mapping/electrophysiological reports (30), indicating that the majority of neurons indeed experienced an intense period of input activity, presumably emanating from layer 4 neurons.

Taken together, our work demonstrates that a SARE reporter, both in vitro and in vivo, can readily trace and mark an ensemble of cells that have experienced intense activity in the recent past. Further works are ongoing to design novel pharmacogenetical and

optogenetical experiments using SARE as a driver for conditional Cre recombinase such as hormone-activated CreER^{T2} (31), or for channelrhodopsins/halorhodopsins (32), with a view to manipulating specific gene expression or neuronal excitability in an activated ensemble of neurons within a circuit.

Materials and Methods

Plasmids, Lentiviruses, and Reagents. Reporter plasmid construction, lentiviral vector preparation, and reagents are described in *SI Materials and Methods*.

Neuronal Culture Preparation, Luciferase Reporter Assay, Fluorescent Protein Reporter Assay, and Luciferase Live-Cell Imaging. Dissociated neuronal culture was prepared from rat embryonic neocortex or postnatal hippocampus as described previously (10, 33). For luciferase assay, cortical neurons were transfected with a firefly luciferase reporter plasmid and an internal control Renilla luciferase plasmid by electroporation. At 10 days in vitro (div), the cells were silenced with TTX for 12–24 h, stimulated with a 4-aminopyridine/bicuculline (4AP/BIC) mixture for 4 h, and lysed. Luciferase activities were measured using the Dual Luciferase assay system (Promega).

For lentiviral reporter assay, hippocampal neurons cultured on coverslips were infected with lentiviruses at 2 div. At 15 div, neurons were silenced with TTX and then stimulated with BDNF (a gift from Dainippon Sumitomo Pharma, Osaka, Japan). For luciferase live-cell imaging, hippocampal neurons transfected with the Arc7000-ELuc-PEST plasmid were imaged in a culture medium containing d-luciferin (0.5 mM, Toyobo) at 14–18 div.

All animal experiments were carried out in accordance with regulations and guidelines of the University of Tokyo and approved by the institutional review committee of University of Tokyo Graduate School of Medicine. More information is provided in *SI Materials and Methods*.

Electrophoretic Mobility Shift Assay (EMSA) and Chromatin Immunoprecipitation (ChIP) Assay. Preparation of brain nuclear extracts is described in *SI Materials and Methods*. The nuclear extracts (2 μg for CREB and SRF and 10 μg for MEF2) were reacted with ^{32}P-radiolabeled DNA probes. Excess amounts (300-fold) of unlabeled probes were added to the reaction mixture for competition assay. Protein-DNA complexes were separated on acrylamide gels and analyzed by an image analyzer (BAS2500, Fujifilm).

Chromatin immunoprecipitation was performed using a kit (Active Motif) essentially following the manufacture's instructions. Precipitates were analyzed using a real-time PCR system (Roche) and gel electrophoresis. More information is provided in *SI Materials and Methods*.

Viral Reporter Assay in Mouse Visual Cortex. Production of lentivirus-infected mice is described in *SI Materials and Methods*. After 3–4 postnatal weeks, the infected mice were subjected to monocular deprivation, dark reared for 1–3 days, exposed to a bright environment for 2–3 h, and then perfused for immunohistochemical analysis. For quantification, infected neurons were identified by native RFP signals and TSA-enhanced GFP-immunoreactive cells were counted. More information is provided in *SI Materials and Methods*.

Statistical Analysis. Statistical analyses were performed using Prism 4.0 (Graphpad Software). Student's paired *t* test and 1-way analysis of variance with repeated measures (ANOVA) followed by Tukey's post hoc test were used for comparisons between 2 groups and 3 groups, respectively. Mann-Whitney *U* test was used for fluorescence reporter assay. All data are shown as mean ± standard error of the mean (SEM), unless otherwise stated.

ACKNOWLEDGMENTS. We thank H. Miyoshi and D. Trono for the lentiviral vector and packaging constructs, respectively; Dainippon Sumitomo Pharma (Osaka, Japan) for supply of BDNF through the courtesy of C. Nakayama and T. Ishiyama; C. Tohyama, M. Kakeyama, and W. Yoshioka (University of Tokyo) for technical help in qPCR analyses; T. Furukawa (Olympus-Japan) for assistance in building a live luciferase imaging microscope. We also thank all members of the Bito laboratory for support and discussion. We are particularly indebted to K. Saiki, Y. Kondo, and T. Kinbara for assistance. This work was supported in part by grants-in-aid from the Ministry of Education, Culture, Sports, Science and Technology (to H.O., M.O., S.T.-K., and H.B.) and from the Ministry of Health, Labor and Welfare (to H.O. and H.B.), by 21st century Center of excellence (COE) and Global COE programs (to H.B.), by a grant from National Institute of Mental Health (MH053608 to P.F.W.), and by awards from the Human Frontier Science Program Organization (career development award to H.O. and a program grant to H.B.), from the Takeda Foundation, from the Toray Science Foundation, and from the Yamada Science Foundation (to H.B.).

1. Kandel ER (2001) The molecular biology of memory storage: a dialogue between genes and synapses. *Science* 294:1030–1038.
2. Bourtchuladze R, *et al.* (1994) Deficient long-term memory in mice with a targeted mutation of the cAMP-responsive element-binding protein. *Cell* 79:59–68.
3. Ramanan N, *et al.* (2005) SRF mediates activity-induced gene expression and synaptic plasticity but not neuronal viability. *Nat Neurosci* 8:759–767.
4. Tokuyama W, Okuno H, Hashimoto T, Xin Li Y, Miyashita Y (2000) BDNF upregulation during declarative memory formation in monkey inferior temporal cortex. *Nat Neurosci* 3:1134–1142.
5. Morris RG (2006) Elements of a neurobiological theory of hippocampal function: the role of synaptic plasticity, synaptic tagging and schemas. *Eur J Neurosci* 23:2829–2846.
6. Pham TA, Impey S, Storm DR, Stryker MP (1999) CRE-mediated gene transcription in neocortical neuronal plasticity during the developmental critical period. *Neuron* 22:63–72.
7. Bliss TV, Collingridge GL (1993) A synaptic model of memory: long-term potentiation in the hippocampus. *Nature* 361:31–39.
8. Bito H, Deisseroth K, Tsien RW (1997) Ca^{2+}-dependent regulation in neuronal gene expression. *Curr Opin Neurobiol* 7:419–429.
9. West AE, Griffith EC, Greenberg ME (2002) Regulation of transcription factors by neuronal activity. *Nat Rev Neurosci* 3:921–931.
10. Bito H, Deisseroth K, Tsien RW (1996) CREB phosphorylation and dephosphorylation: a Ca($^{2+}$)- and stimulus duration-dependent switch for hippocampal gene expression. *Cell* 87:1203–1214.
11. Robertson LM, *et al.* (1995) Regulation of c-fos expression in transgenic mice requires multiple interdependent transcription control elements. *Neuron* 14:241–252.
12. Flavell SW, Greenberg ME (2008) Signaling mechanisms linking neuronal activity to gene expression and plasticity of the nervous system. *Annu Rev Neurosci* 31:563–590.
13. Link W, *et al.* (1995) Somatodendritic expression of an immediate early gene is regulated by synaptic activity. *Proc Natl Acad Sci USA* 92:5734–5738.
14. Lyford GL, *et al.* (1995) Arc, a growth factor and activity-regulated gene, encodes a novel cytoskeleton-associated protein that is enriched in neuronal dendrites. *Neuron* 14:433–445.
15. Plath N, *et al.* (2006) Arc/Arg3.1 is essential for the consolidation of synaptic plasticity and memories. *Neuron* 52:437–444.
16. Shepherd JD, *et al.* (2006) Arc/Arg3.1 mediates homeostatic synaptic scaling of AMPA receptors. *Neuron* 52:475–484.
17. Chowdhury S, *et al.* (2006) Arc/Arg3.1 interacts with the endocytic machinery to regulate AMPA receptor trafficking. *Neuron* 52:445–459.
18. Guzowski JF, *et al.* (2000) Inhibition of activity-dependent arc protein expression in the rat hippocampus impairs the maintenance of long-term potentiation and the consolidation of long-term memory. *J Neurosci* 20:3993–4001.
19. Guzowski JF, McNaughton BL, Barnes CA, Worley PF (1999) Environment-specific expression of the immediate-early gene Arc in hippocampal neuronal ensembles. *Nat Neurosci* 2:1120–1124.
20. Han JH, *et al.* (2007) Neuronal competition and selection during memory formation. *Science* 316:457–460.
21. Tagawa Y, Kanold PO, Majdan M, Shatz CJ (2005) Multiple periods of functional ocular dominance plasticity in mouse visual cortex. *Nat Neurosci* 8:380–388.
22. Ramirez-Amaya V, *et al.* (2005) Spatial exploration-induced Arc mRNA and protein expression: evidence for selective, network-specific reactivation. *J Neurosci* 25:1761–1768.
23. Waltereit R, *et al.* (2001) Arg3.1/Arc mRNA induction by Ca^{2+} and cAMP requires protein kinase A and mitogen-activated protein kinase/extracellular regulated kinase activation. *J Neurosci* 21:5484–5493.
24. Li L, Carter J, Gao X, Whitehead J, Tourtellotte WG (2005) The neuroplasticity-associated arc gene is a direct transcriptional target of early growth response (Egr) transcription factors. *Mol Cell Biol* 25:10286–10300.
25. Wallace CS, Lyford GL, Worley PF, Steward O (1998) Differential intracellular sorting of immediate early gene mRNAs depends on signals in the mRNA sequence. *J Neurosci* 18:26–35.
26. Thomas GM, Huganir RL (2004) MAPK cascade signalling and synaptic plasticity. *Nat Rev Neurosci* 5:173–183.
27. Hashimoto M, Mikoshiba K (2004) Neuronal birthdate-specific gene transfer with adenoviral vectors. *J Neurosci* 24:286–296.
28. Flavell SW, *et al.* (2006) Activity-dependent regulation of MEF2 transcription factors suppresses excitatory synapse number. *Science* 311:1008–1012.
29. Davis FJ, Gupta M, Camoretti-Mercado B, Schwartz RJ, Gupta MP (2003) Calcium/calmodulin-dependent protein kinase activates serum response factor transcription activity by its dissociation from histone deacetylase, HDAC4. Implications in cardiac muscle gene regulation during hypertrophy. *J Biol Chem* 278:20047–20058.
30. Bear MF, Kleinschmidt A, Gu QA, Singer W (1990) Disruption of experience-dependent synaptic modifications in striate cortex by infusion of an NMDA receptor antagonist. *J Neurosci* 10:909–925.
31. Feil R, Wagner J, Metzger D, Chambon P (1997) Regulation of Cre recombinase activity by mutated estrogen receptor ligand-binding domains. *Biochem Biophys Res Commun* 237:752–757.
32. Zhang F, Aravanis AM, Adamantidis A, de Lecea L, Deisseroth K (2007) Circuit-breakers: optical technologies for probing neural signals and systems. *Nat Rev Neurosci* 8:577–581.
33. Takemoto-Kimura S, *et al.* (2007) Regulation of dendritogenesis via a lipid-raft-associated Ca^{2+}/calmodulin-dependent protein kinase CLICK-III/CaMKIgamma. *Neuron* 54:755–770.

Supporting Information

Kawashima *et al.* 10.1073/pnas.0806518106

SI Materials and Methods

Plasmid Construction. Genomic fragments containing 5′ UTR and the regulatory region of the *Arc/Arg-3.1* gene were amplified by PCR from a 129/Sv strain mouse bacterial artificial chromosome (BAC, clone24533, Incyte Genomics), and subcloned into the XhoI/BglII sites of a firefly luciferase reporter plasmid pGL4.11[luc2P] (Promega). Detailed genomic positions of each genomic fragment were as follows: −1000 (≈ −996 to +198), −2000 (−1996 to +198), −3000 (−2996 to +198), −4000 (−3996 to +198), −5000 (−4996 to +198), and −7000 (−7065 to +198), where +1 denotes the transcription initiation site. The resulting reporter plasmid harboring the −1000 fragment was designated as pGL4.11-Arc1000-luc2P, and a similar nomenclature was used with other reporter plasmids. The pGL4.11-Arc7000-del no. 1-luc2P and pGL4.11-Arc7000-del no. 2-luc2P plasmids were created by excising fragments between an SwaI site (−6668) and a XhoI site (−7065), and a Tth111I site (−6894) and the XhoI site, of the pGL4.11-Arc7000-luc2P, respectively. To directly examine the enhancer activity of SARE (Figs. 3 and 4), two distinct TATA-containing minimum promoter plasmids, pGL4.11-ArcMin-luc2P and pGL4.11-minCMV-luc2P, were constructed by inserting the ArcMin fragment, which contains a short upstream sequence and 5′ UTR (−222 to +198) of the *Arc* gene, and the minCMV fragment (1), which corresponds to the minimum sequence (−51 to +6) of the CMV IE promoter, into the BglII/HindIII sites of pGL4.11[luc2P], respectively. The SARE fragment (−6793 to −6690) was further subcloned into the XhoI/BglII sites of pGL4.11-ArcMin-luc2P and pGL4.11-minCMV-luc2P, thus creating pGL4.11-SARE-ArcMin-luc2P and pGL4.11-SARE-minCMV-luc2P, respectively. For mutation analyses of SARE (Fig. 4), point mutations were introduced into pGL4.11-Arc7000-luc2P and pGL4.11-SARE-minCMV-luc2P by PCR-based mutagenesis using the following primers: box *A*, 5′-ctgagccatgacgcagcaaggcgctt*a*ccc*a*agcaggaaggctctgtgcgctg-3′; box *B*, 5′-gaggctgagaatagctgagccatg*ttt*cagcaaggagcttccccacgcag-3′; box *C*, 5′-ccggcaccataaaaggagagaggc*g*gag*c*ata*t*ctgagccatgacg-cagcaag-3; and box *D*, 5′-gcagcctgcctgcttccggcac*a*ata-*c*aag*t*agagaggctgagaatagctga-3′; where bold and italic characters denote mutated sites.

To create d2EGFP reporter plasmids, a destabilized EGFP (d2EGFP) cDNA fragment was excised from pTAL-d2EGFP (Clontech) and replaced with the luc2P fragment of pGL4.11[luc2P]. The resulting plasmid was designated as pGL4.11-d2EGFP, and Arc4000, Arc7000, ArcMin, and SARE-ArcMin fragments described above were further subcloned into the XhoI/BglII sites of the pGL4.11-d2EGFP. Arc7000-ELuc-PEST (Emerald Luc-PEST) plasmid was created by inserting the Arc7000 fragment into the XhoI/BglII sites of pELuc(PEST)-test (Toyobo).

Genomic positions noted above were numbered according to the NCBI mouse genome database (Build 37.1). All plasmid constructs were verified by sequencing.

Reagents. Tetrodotoxin (TTX) (Wako), 4-aminopyridine (4-AP) (Sigma), water-soluble bicuculline (BIC) (Tocris), strychnine (Sigma), glycine (Nacalai Tesque), water-soluble 6-cyano-7-nitroquinoxaline-2,3-dione (CNQX) (Tocris), and D-(-)-2-amino-5-phosphonopentanoic acid (D-AP5) (Tocris) were dissolved in water, and KN-92 (Merck), KN-93 (Merck), U0124 (Merck), and U0126 (Merck) were dissolved in dimethyl sulfoxide (DMSO) (Sigma) to make 500-1000 x stock solutions. All other chemicals were purchased from Nacalai, unless otherwise stated.

Sequence Homology Analysis and Transcription Factor Binding Site Prediction. Genomic sequences surrounding the *Arc/Arg-3.1* gene of various species were obtained from the NCBI genome database (Gene ID: mouse, 11838; rat, 54323; cow, 519403; macaque, 702690; human, 23237; opossum, 12632237; platypus, 149410163). The cavy sequence was obtained from genomic sequence AAKN02023196. For pairwise comparison of the mouse and human *Arc/Arg-3.1* promoters, genomic regions 10 kb upstream of the transcription initiation site were aligned using the mVISTA/AVID alignment program (2, 3). Local sequence comparison around SARE of multiple species was done using the AlignX (ClustalW) program in the VectorNTI Suite 9 software (Invitrogen). The dendrogram was drawn with the Njprot program. Putative transcription factor binding sites were identified with the help of the MatInspector program (Genomatix Software).

Immunocytochemistry and Western Blotting. For immunostaining of endogenous Arc, cortical neurons were stimulated as for the luciferase assay. After stimulation, cells were fixed and immunostained essentially as described previously (4). The primary antibodies used were a mouse anti-luciferase mAb (C-21, Santa Cruz) (1:200) and a rabbit anti-Arc pAb (OP-1, 1:2000) that was raised against bacterially expressed recombinant GST-fused full-length Arc (Okuno *et al.*, unpublished data). The secondary antibodies were AlexaFluor594- or AlexaFlour488-conjugated anti-rabbit and anti-mouse antibodies (1:1000) (Invitrogen).

Western blotting was performed essentially as described previously (4). Cells were lysed in a sample buffer and separated on a standard discontinuous acrylamide gel (10%) or a gradient acrylamide gel (4−12%) (Invitrogen). The primary antibodies used were a mouse anti-β-tubulin mAb (TUB2.1) (Sigma) and the rabbit anti-Arc pAb. The secondary antibodies were HRP-conjugated anti-mouse and anti-rabbit antibodies (GE Healthcare). Chemiluminescence was detected using ECL-Plus reagent (GE Healthcare) and a LAS4000mini image analyzer (Fujifilm).

Luciferase Reporter Assay. Cortical neurons were transfected with a firefly luciferase reporter plasmid and an internal control Renilla luciferase plasmid pGL4.74 [hRluc/TK] (Promega) at a ratio of 4:1 (0.60 μg and 0.15 μg for each well) by electroporation using a Nucleofector (Amaxa) and plated at a density of 1.25×10^6 cells in a 12-well dish. At 10 days in vitro (div), the cells were pretreated with a medium containing 2 μM TTX. After 12–24 h (i.e., 11 div), cells were stimulated with a medium containing 100 μM 4-aminopyridine (4AP), 30 μM bicuculline (BIC), 100 μM glycine, and 1 μM strychnine. For analyses of signaling pathways (Fig. S5), kinase inhibitors and channel blockers were added to the medium 30 min before the stimulation. Cells were lysed 4 h after stimulation, and luciferase activities of both firefly and renilla were measured using the Dual Luciferase assay system (Promega) and a Fluoroskan Ascent FL luminometer (Thermo Fisher Scientific), according to the manufacturers' protocols. The firefly luciferase activities were normalized with the intra-sample renilla luciferase activities, corrected for transfected plasmid copy numbers, and further normalized to an arbitrary standard value (Arc1000 in TTX) for appropriate comparison of different reporter plasmids. Assays using different batches of neuronal culture (i.e., primary culture prepared

from different animals on different days) were regarded as independent experiments.

Fluorescent Protein Reporter Assay. Hippocampal neurons cultured on coverslips were cotransfected with a d2EGFP reporter plasmid and a marker plasmid pTagRFP-C (Evrogen) at a ratio of 5:1 using Lipofectamine 2000 (Invitrogen) at 7 div. Neurons were pretreated with a medium containing TTX at 15 div, and stimulated with a medium containing 4AP/BIC/glycine/strychnine at 16 div as for the luciferase assay. After 4 h, cells were fixed and mounted on slides. The average GFP intensity in the soma of all RFP-positive neurons was quantified.

To evaluate the reporter activity of SARE-ArcMin lentivirus, hippocampal neurons (2 div) cultured on coverslips were infected with SARE-ArcMin lentivirus at a MOI of about 1. Neurons were pretreated with 2 μM TTX at 15 div and stimulated at 16 div with 50 ng/ml BDNF (generously provided by Dainippon Sumitomo Pharma through the courtesy of Dr. Chikao Nakayama). After 5–6 h, cells were fixed and mounted on slides.

Nuclear Extract Preparation from Stimulated Cerebral Cortex. Eight-week-old male Wistar rats were given electrical shocks (100 V, 5 msec, 100 Hz for 5 sec) through ear clips connected to an electrical stimulator (SIU-102, Warner Instruments) controlled by a pulse generator (Master-8, A.M.P.I.) and killed after 30–40 min. The brains were rapidly removed, and the neocortex was dissected. Nuclear extracts were isolated essentially as described previously (5), except that protease and phosphatase inhibitor cocktails, Complete and PhosStop (Roche Diagnostics), were added in extraction buffers. The resulting protein extracts were desalted using Amicon Ultra-15 filter devices (Millipore) in a buffer [20 mM Hepes (pH 7.6), 150 mM KCl, 1 mM EDTA, 1.5 mM $MgCl_2$, 1 mM DTT, 10% glycerol] and stored at −80 °C. Protein concentrations were measured by the Quick Start Bradford Protein Assay (Bio-Rad).

Electrophoretic Mobility Shift Assay. For protein-DNA binding reaction, 2 μg (for CREB and SRF) or 10 μg (for MEF2) of nuclear extracts were reacted with a ^{32}P-radiolabeled DNA probe (see below) in a 20-μL reaction mixture [25 mM Hepes (pH 7.6), 60 mM KCl, 1 mM EDTA, 5 mM $MgCl_2$, 1 μg poly(dI-dC), 0.1 μg poly L-lysine, 10% glycerol]. For competition assay, the mixture was reacted in the presence of excess amounts (300-fold) of unlabeled probes. For supershift assay, anti-CREB mAb (48H2, Cell Signaling), anti-MEF2D mAb (clone 9, BD Biosciences), anti-SRF pAb (H-300x, Santa Cruz), and control anti-Myc mAb (9B11, Cell Signaling) were added to the reaction mixture. Essentially the same results were obtained using different anti-CREB (E306, Epitomics), anti-MEF2 (H-300x, Santa Cruz), and anti-SRF (ab53130, Abcam) antibodies. The mixtures were incubated for 15 min at room temperature, and the resulting protein-DNA complexes were separated by electrophoresis on a 5% nondenaturing acrylamide gel in 0.25 × TBE buffer. The gels were dried, exposed overnight to a BAS-SR2040 imaging plate (Fujifilm), and analyzed by the BAS2500 image analyzer (Fujifilm).

The DNA probes used were the followings:
box *B*, 5′-ACATACTTGCTGCGTCATGGCTCAGAGATG-3′;
mutB, 5′-ACATACTTGCTG*AAA*CATGGCTCAGAGATG-3′;
box *C*, 5′-ATTGGCTCAGCTATTCTCAGCCTCTCTACG-3′;
mutC, 5′-ATTGGCTCAG*A*TAT*G*CTCC*G*CCTCTCTACG-3′;
box *D*, 5′-AATCCTCTCTCCTTTTATGGTGCCGTCGGC-3′;
mutD, 5′-AATCCTCTCT*A*CTT*G*TAT*T*GTGCCGTCGGC-3′;
where italic characters denote mutated nucleotides.

The analysis of MEF2-box*C* complex required relatively large amounts of nuclear extracts, which inevitably brought higher nonspecific signals. To reduce these nonspecific signals, mutated competitors were added to the reaction in MEF2-antibody supershift assays.

Chromatin Immunoprecipitation (ChIP) Assay. Cortical neurons were cultured on a 10-cm dish at a density of 1.25×10^7 cells/dish. At 13–15 div, the neurons were treated with 1 μM TTX overnight and stimulated with the 4AP/BIC mixture for 30 min. The chromatin immunoprecipitation assay was performed using the ChIP-IT Express kit (Active Motif) according to the manufacturer's instructions with some modifications. Briefly, the neurons were fixed with 1% PFA in a culture medium for 10 min at room temperature, homogenized, and centrifuged. The pellets were resuspended in a shearing buffer and sheared using a cup-horn sonicator (XL2020/431A, Misonix Inc.) with ice-cold water perfusion. The sonication-sheared lysates were cleared by centrifugation and used for chromatin immunoprecipitation. The quality of shearing was monitored by DNA electrophoresis for each shearing batch. We only used the sheared chromatin lysates in which the length of DNA fragments were ranging from 200 to 1000 bp with an average of ≈500 bp. The sheared chromatin lysates (50–60 μg proteins) were reacted with a specific antibody (1–2 μg) overnight at 4 °C and immunoprecipitated with protein G magnetic beads. The precipitated DNA-chromatin complex was washed, eluted, incubated for 6 h at 65 °C in a reverse cross-link buffer, and digested with proteinase K for 1 h at 37 °C. The resultant DNA was purified using a purification column. Antibodies used for immunoprecipitation were the following: rabbit polyclonal anti-CREB and control IgG (ChIPAb+ CREB kit, Millipore), rabbit polyclonal anti-SRF (sc-335X, Santa Cruz), mouse monoclonal anti-MEF2D (BD Biosciences), and control IgG (ChIP-IT control kit, Active Motif).

The precipitated DNA fractions were analyzed using a real-time PCR system (Light Cycler 1.5, Roche) with SYBR Green I kits (TaKaRa and Roche). The primers used were: SARE primers set 1 (−6778 to −6649, for CREB and MEF2), 5′-ggctggctctgggaggtattta-3′ and 5′-cccccagagatgagagttcaga-3′; SARE primers set 2 (−6815 to −6649, for SRF), 5′-ctccttttatggtgccggaag-3′ and 5′-cccccagagatgagagttcaga-3′; negative control primers (+2904 to +3149, in *Arc/Arg-3.1* 3′-UTR locus), 5′-agaaccttgcaggagcctta-3′ and 5′-atggaggaacctcaacatgg-3′; somatostatin primers (−142 to +37), 5′- tgcgaggctaatggtgcg-taaa-3′ and 5′-cttgagcgcggtgggtcagt-3′; Nur77 primers (−547 to −364), 5′-gtccgggactgactgggaaa-3′ and 5′-gtcccggggtccgaaataac-3′; β-actin primers (+14 to +232), 5′-cacccgcgagtacaaccttctt-3′ and 5′-caccctaggcggaaagttaagc-3′. The PCR products were visualized by electrophoresis in 4% agarose gels (NuSieve 3:1, Lonza). The identity of each product was confirmed by restriction enzyme digestion.

Reanalysis of Recently Published SRF ChIP-Seq Raw Data Confirmed the Potential of SRF Binding to the SARE Sequence (6).

Live Imaging. For luciferase live-cell imaging, hippocampal neurons plated on glass-bottom dishes were cotransfected with the Arc7000-ELuc-PEST plasmid and a marker plasmid pEGFP-C1 (Clontech) at 7 div as described before. At 14–18 div, neurons were incubated in a culture medium containing d-luciferin (0.5 mM, Toyobo) at 37 °C in a stage CO_2 chamber (Tokai Hit). Transfected neurons were identified by GFP signals, and luminescent images were acquired with 5-min exposure every 60 min. After collecting baseline images, neurons were stimulated by field-electrical pulses (3 ms, 50 mA, 100 pulses at 100 Hz, 10 times with 30-sec intervals) from 2 parallel platinum electrodes using an electrical stimulator (SIU-102, Warner Instruments) controlled by a pulse generator (Master-8, A.M.P.I.) (7). The integrated luminescence in the soma (L) of individual neurons was normalized to the basal luminescence (L_0) before the stimulation.

Lentivirus Vector Construction and Viral Production. A lentiviral SARE-ArcMin reporter plasmid (CS-SARE-ArcMin-d2EGFP)

was created by introducing 2 independent expression cassettes, SARE-ArcMin-d2EGFP (GFP, activity reporter) and PGK-TurboFP635 (RFP, infection marker), into a lentiviral plasmid CS-CA-MCS (8). These 2 cassettes were placed in the opposite directions, and an intermediate insulator sequence was placed to prevent interactions between the cassettes (9). To insert multiple fragments, the chicken actin-promoter fragment of the lentiviral plasmid CS-CA-MCS (generously provided by Dr. Hiroyuki Miyoshi, RIKEN-BRC, Japan) was excised by PstI/XhoI digestion and replaced with a synthetic oligonucleotide 5′-tgaattcttcgaactgcagggcgcgccgctagcaccggtctcgaggttaacggatccg-3′, which contains (EcoRI-BstBI-PstI-AscI-NheI-AgeI-XhoI-HpaI-BamHI) unique restriction enzyme sites. A synthetic oligonucleotide containing the enhancer blocking FII sequence from the chicken β-globin insulator (10) 5′-cgcgccgccccgggcg-gctcgctgctgccccctagcgggggagg-gacgtaattacatccctgggggctttgggggggg-3′ was inserted into the AscI/NheI sites. The mouse phosphoglycerate kinase (PGK) promoter and TurboFP635 cDNA (Evrogen) were amplified by PCR and subcloned into the XhoI/HpaI sites and the HpaI/BamHI sites, respectively. The destabilized EGFP (d2EGFP) cDNA with SV40 polyA sequence were amplified from pTAL-d2EGFP (Clontech) and subcloned into the BstBI/EcoRI sites. The SARE-ArcMin fragment was subcloned into the AscI/BstBI sites, thus creating CS-SARE-ArcMin-d2EGFP. A control lentiviral plasmid, CS-ArcMin-d2EGFP, was created by the same process as described above, except that the ArcMin fragment was inserted instead of the SARE-ArcMin.

To generate self-inactivating lentiviruses, CS-SARE-ArcMin-d2EGFP or CS-ArcMin-d2EGFP were cotransfected with ps-PAX2 (Addgene plasmid 12260) and pMD2.G (Addgene plasmid 12259) (courtesy of Dr. Didier Trono, EPFL, Switzerland) into HEK293T cells using the calcium phosphate method. Culture supernatants were collected 48−72 h after transfection, filtered with 0.45 μm cellulose acetate membrane filters (Asahi Techno Glass), and ultracentrifuged at 80,000 × *g* for 2 h. The resulting pellets were dissolved in PBS to obtain concentrated virus solutions. Virus titer was determined using HEK293T cells by counting RFP-positive cells.

Live Imaging of Lentivirus-Infected Neurons. Hippocampal neurons cultured on glass-bottom dishes were infected at 7–8 div with the SARE-ArcMin reporter or the ArcMin control lentiviruses at a nominal MOI of 2–12. After 1–2 weeks, neurons were incubated in a stage CO_2 chamber (Tokai Hit) and fluorescent images were acquired every 20 min. Neurons were stimulated by field electrical pulses (3 ms, 100 mA, 100 pulses at 100 Hz, 9 times with 1-min intervals). The GFP and RFP fluorescence in the soma of individual neurons was monitored before and after the stimulation. GFP fluorescence was divided by RFP fluorescence (F) and further normalized to the basal fluorescence (F_0) before the stimulation.

Viral Reporter Assay in Mouse Visual Cortex. Injection of lentiviruses into mouse embryos in the uterus was performed similarly to the procedure previously reported for in vivo electroporation (11, 12). Virus solutions (1–2 μL) were injected into the lateral ventricle of E15 embryos in the uterus. The pups were born naturally and grew without any apparent abnormality.

After 3–4 postnatal weeks, the pups were subjected to monocular deprivation by suture and glue. The pups were subsequently dark reared for 1–3 days, and exposed to a bright environment for 2–3 h. The pups were then perfused with 4% paraformaldehyde/phosphate buffer. The brains were removed, postfixed, cryoprotected, and frozen in M1 Embedding Matrix (Shandon, Thermo Scientific). Coronal sections (30 μm) of the visual cortex were cut using a cryostat. The primary visual cortex was defined according to a brain atlas (13).

Immunohistochemistry was performed as previously described (5, 14, 15), except that the TSA system was used for detection. The sections were treated with a rabbit anti-GFP pAb (A-11122, 1:3000) (Invitrogen). After washing, the sections were treated with an HRP-conjugated anti-rabbit goat pAb (1:500, Jackson Immunoresearch), and the signals were developed using a TSA Plus FITC System (PerkinElmer) according to the manufacturer's protocols. A subset of sections were immunostained with a rat anti-GFP mAb (GF090R, Nacalai) and an anti-rat AlexaFlour488-conjugated antibody.

Infected neurons in the primary visual cortex were identified by native RFP signals. GFP immunoreactivity-positive cells were counted, and the ratio of the number of RPF/GFP double-positive cells to the RFP-positive cells was calculated for each hemisphere of individual brains. The binocular areas were excluded from the regions of interest. Endogenous Arc/Arg-3.1 induction in the visual cortex was confirmed by staining sections with a rabbit anti-Arc pAb (OP-2, 1:2000, Okuno *et al.*, unpublished data).

Image Acquisition. The fluorescence protein reporter assay used a 40× objective (NA 1.3, Oil) with an EM-CCD camera (iXon, Andor Technology) attached to an inverted microscope (IX81, Olympus, Tokyo, Japan). Luciferase live-cell imaging and fluorescence live-cell imaging used a 40x objective (NA 0.95, Air) with the Andor CCD camera. Fixed fluorescent images of lentivirus-infected cultured neurons and mouse visual cortex were obtained using a 20× objective (NA 0.65, Air) with a color CCD camera (DP-70, Olympus) attached to an upright microscope (BX-51, Olympus) or a 20× objective (NA 0.5) with a confocal laser microscopy system (LSM 510META-V3.2, Carl Zeiss) attached to an inverted microscope (Axiovert 200M). Collected images were analyzed using Metamorph software (Molecular Devices) or ImageJ software (National Institutes of Health).

1. Gossen M, *et al.* (1995) Transcriptional activation by tetracyclines in mammalian cells. *Science* 268:1766–1769.
2. Frazer KA, Pachter L, Poliakov A, Rubin EM, Dubchak I (2004) VISTA: computational tools for comparative genomics. *Nucleic Acids Res* 32:W273–279.
3. Bray N, Dubchak I, Pachter L (2003) AVID: a global alignment program. *Genome Res* 13:97–102.
4. Takemoto-Kimura S, *et al.* (2007) Regulation of dendritogenesis via a lipid-raft-associated Ca^{2+}/calmodulin-dependent protein kinase CLICK-III/CaMKIgamma. *Neuron* 54:755–770.
5. Okuno H, Saffen DW, Miyashita Y (1995) Subdivision-specific expression of ZIF268 in the hippocampal formation of the macaque monkey. *Neuroscience* 66:829–845.
6. Valouev A, *et al.* (2008) Genome-wide analysis of transcription factor binding sites based on ChIP-Seq data. *Nat Methods* 5:829–834.
7. Furuyashiki T, Arakawa Y, Takemoto-Kimura S, Bito H, Narumiya S (2002) Multiple spatiotemporal modes of actin reorganization by NMDA receptors and voltage-gated Ca^{2+} channels. *Proc Natl Acad Sci USA* 99:14458–14463.
8. Miyoshi H, Blomer U, Takahashi M, Gage FH, Verma IM (1998) Development of a self-inactivating lentivirus vector. *J Virol* 72:8150–8157.
9. Vogel R, Amar L, Thi AD, Saillour P, Mallet J (2004) A single lentivirus vector mediates doxycycline-regulated expression of transgenes in the brain. *Hum Gene Ther* 15:157–165.
10. Bell AC, West AG, Felsenfeld G (1999) The protein CTCF is required for the enhancer blocking activity of vertebrate insulators. *Cell* 98:387–396.
11. Saito T, Nakatsuji N (2001) Efficient gene transfer into the embryonic mouse brain using in vivo electroporation. *Dev Biol* 240:237–246.
12. Tabata H, Nakajima K (2001) Efficient in utero gene transfer system to the developing mouse brain using electroporation: visualization of neuronal migration in the developing cortex. *Neuroscience* 103:865–872.
13. Franklin K, Paxinos G (1997) *The Mouse Brain in Stereotaxic Coordinates* (Academic, New York).
14. Okuno H, Kanou S, Tokuyama W, Li YX, Miyashita Y (1997) Layer-specific differential regulation of transcription factors Zif268 and Jun-D in visual cortex V1 and V2 of macaque monkeys. *Neuroscience* 81:653–666.
15. Okuno H, Miyashita Y (1996) Expression of the transcription factor Zif268 in the temporal cortex of monkeys during visual paired associate learning. *Eur J Neurosci* 8:2118–2128.

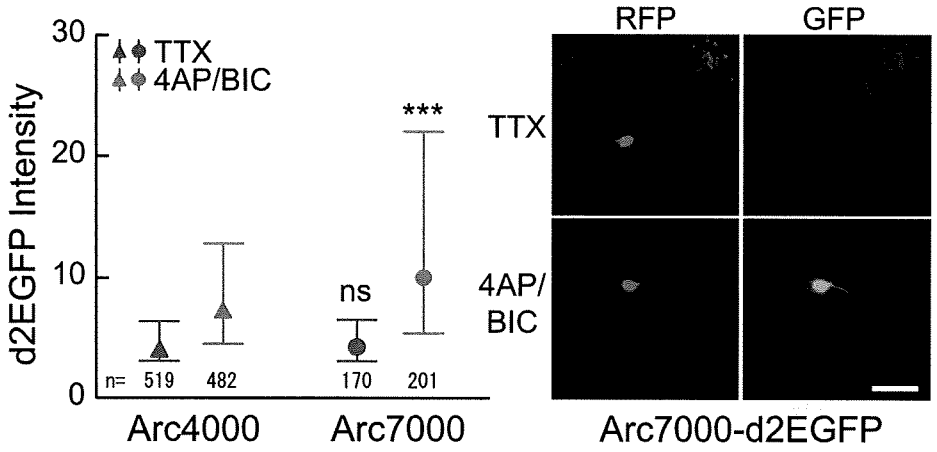

Fig. S1. Activation of Arc7000 in individual hippocampal neurons. Neurons were cotransfected with reporter (d2EGFP) and transfection marker (tagRFP) plasmids, stimulated with 4AP/BIC, and average GFP fluorescence in the soma was quantified. The triangles and circles represent median values, and bars represent quadrant points. Representative images of Arc7000 transfected neurons are shown on the *Right*. GFP reporter signals were more elevated after stimulation downstream of Arc7000 than of Arc4000. The difference between Arc7000 and Arc4000 appeared smaller than that obtained by the luciferase assays, presumably owing to higher background autofluorescence. Numbers in the *Left* panel indicate the number of neurons analyzed. ***, $P < 0.001$; ns, not significant (Mann-Whitney test) compared with the 4AP/BIC or the TTX value of Arc4000. (Scale bar, 50 μm.)

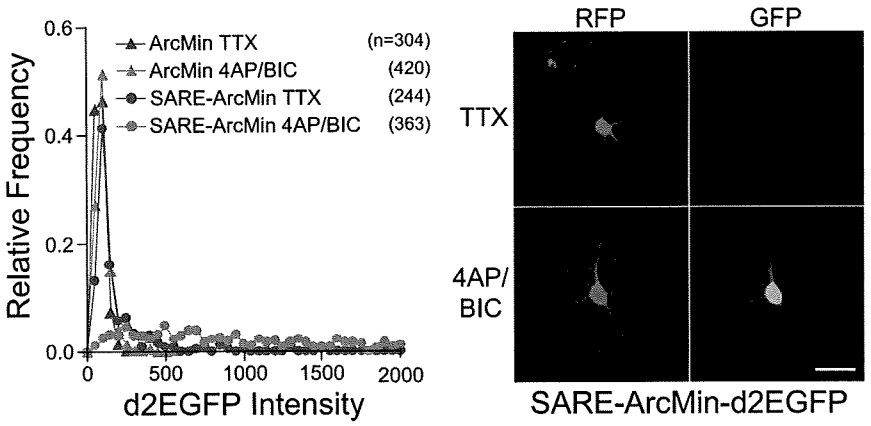

Fig. S2. Activation of SARE in individual hippocampal neurons. Neurons were cotransfected with reporter (d2EGFP) and transfection marker (tagRFP) plasmids, stimulated with 4AP/BIC and average GFP fluorescence in the soma was quantified. The frequency histogram of reporter GFP signals in individual neurons is shown. The distribution of activated GFP signals from SARE-ArcMin was dramatically shifted to the right compared to that from ArcMin alone. Representative images of SARE-ArcMin transfected neurons are shown on the *Right*. Numbers in the *Left* panel indicate the number of neurons analyzed. (Scale bar, 50 μm.)

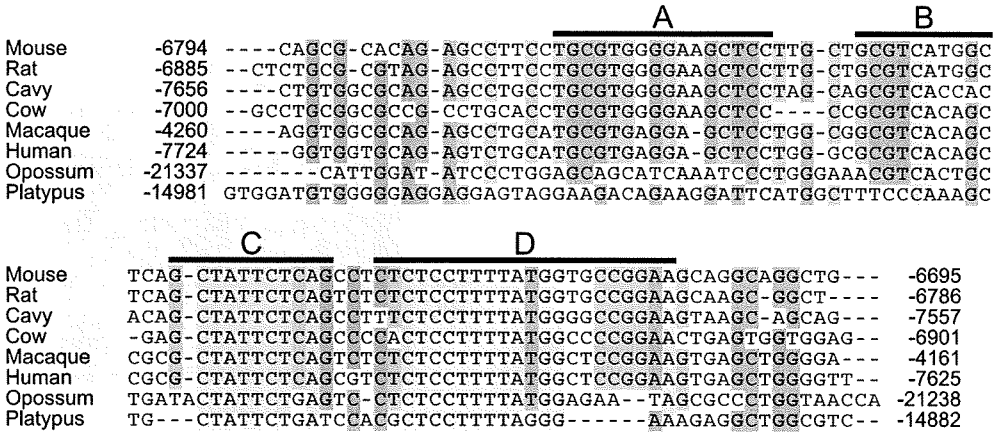

Fig. S3. Divergence of *Arc/Arg-3.1* SARE sequence across various mammalian species.

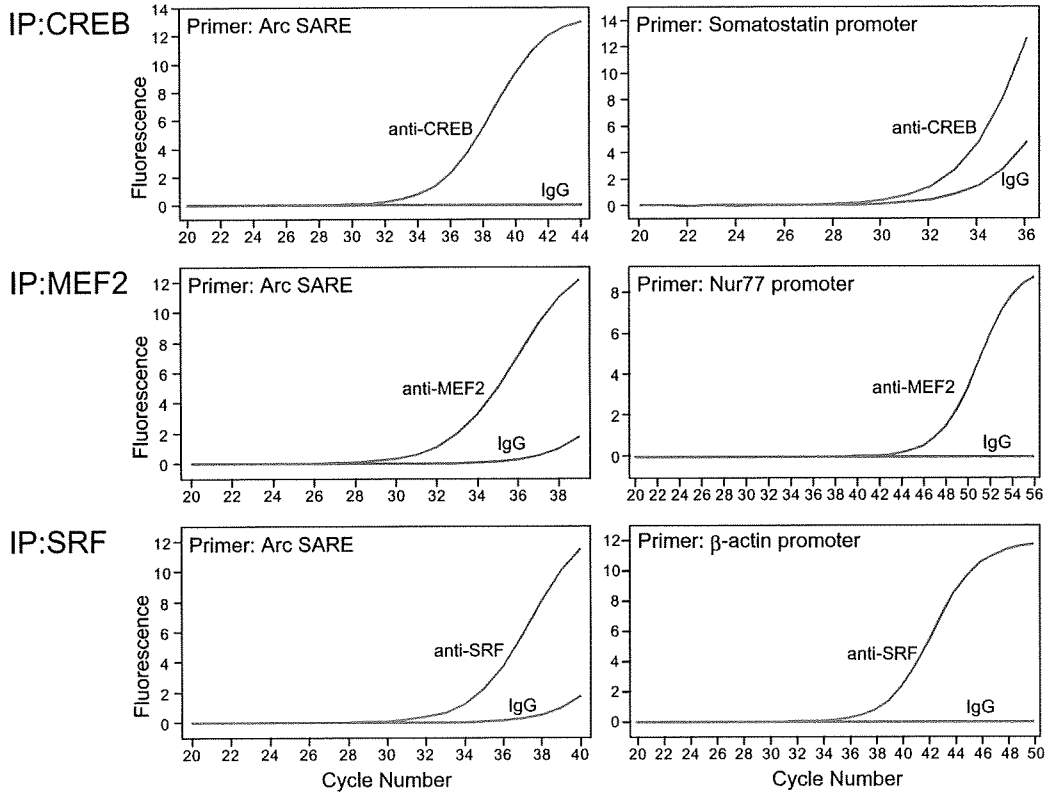

Fig. S4. Representative real-time PCR data of ChIP assays. SYBR Green I fluorescence was plotted against PCR cycle numbers. The chromatin lysates were immunoprecipitated (IP) with antibodies against 3 transcription factors. Genomic fragments in the precipitates were analyzed using specific primers indicated in each panel. The onset of fluorescence increment in the precipitates (red) always preceded that in the control IgG precipitates (blue), indicating the specific binding of CREB, MEF2, and SRF to target genomic sequences. The specificity of the PCR was confirmed by melting curve analyses.

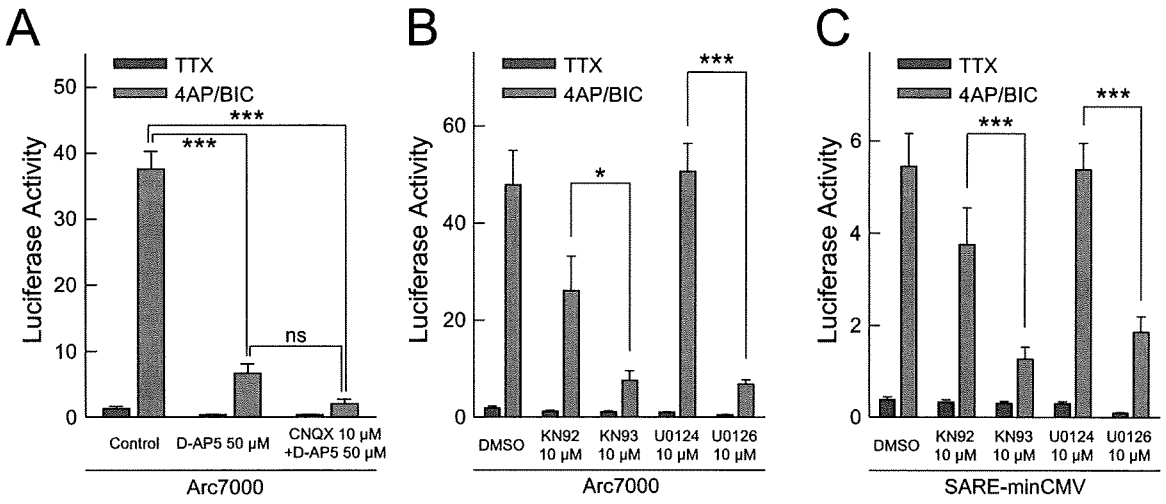

Fig. S5. Pharmacological analysis of the Arc7000- and SARE-activating signaling cascades. (*A*) The activation of Arc7000 is suppressed by ionotropic glutamate receptor antagonists. Activation of Arc7000 was almost completely suppressed when both AMPA-R and NMDA-R were blocked by CNQX and AP5. Activation of Arc7000 was also diminished by 80% when only NMDA-R was blocked. ***, $P < 0.001$; ns, not significant (1-way ANOVA with Tukey's test). (*B* and *C*) The CaMK and MAPK pathways are involved in the activation of Arc7000 via SARE. Neurons were treated with a CaMK inhibitor, KN-93, and a MEK inhibitor, U0126, shortly before and during the 4AP/BIC stimulation and subjected to the luciferase assay. The activation levels (4AP/BIC) of the Arc7000 and the SARE-minCMV activities were significantly diminished by both KN-93 and U0126 compared with their inactive analogues, KN-92 and U0124, respectively. *, $P < 0.05$; ***, $P < 0.001$ (1-way ANOVA with Tukey's test).